american physiological society

JNP JOURNAL OF NEUROPHYSIOLOGY

J Neurophysiol 132: 849–869, 2024.
First published July 25, 2024; doi:10.1152/jn.00164.2024

RESEARCH ARTICLE

Higher Neural Functions and Behavior

Structural covariation between cerebellum and neocortex intrinsic structural covariation links cerebellum subregions to the cerebral cortex

Zilong Wang,[1,2] Jörn Diedrichsen,[3,4,5] Karin Saltoun,[1,2] Christopher Steele,[6,7] Sheeba Rani Arnold-Anteraper,[8,9] B. T. Thomas Yeo,[10] Jeremy D. Schmahmann,[11] and Danilo Bzdok[1,2]

[1]*McConnell Brain Imaging Centre, Department of Biomedical Engineering, Faculty of Medicine, School of Computer Science, The Neuro—Montreal Neurological Institute (MNI), McGill University, Montreal, Quebec, Canada;* [2]*Mila—Quebec Artificial Intelligence Institute, Montreal, Quebec, Canada;* [3]*Western Institute for Neuroscience, Western University, London, Ontario, Canada;* [4]*Department of Computer Science, Western University, London, Ontario, Canada;* [5]*Department of Statistical and Actuarial Sciences, Western University, London, Ontario, Canada;* [6]*Department of Psychology, Concordia University, Montreal, Quebec, Canada;* [7]*Department of Neurology, Max Planck Institute for Human Cognitive and Brain Sciences, Leipzig, Germany;* [8]*Advanced Imaging Research Center, UTSW, Dallas, Texas, United States;* [9]*Department of Bioengineering, University of Illinois Urbana-Champaign, Urbana, Illinois, United States;* [10]*Department of Electrical & Computer Engineering, Centre for Translational MR Research, Centre for Sleep & Cognition, N.1 Institute for Health and Institute for Digital Medicine, National University of Singapore, Singapore, Singapore; and* [11]*Ataxia Center, Cognitive Behavioral Neurology Unit, Laboratory for Neuroanatomy and Cerebellar Neurobiology, Department of Neurology, Massachusetts General Hospital and Harvard Medical School, Boston, Massachusetts, United States*

Abstract

The human cerebellum is increasingly recognized to be involved in nonmotor and higher-order cognitive functions. Yet, its ties with the entire cerebral cortex have not been holistically studied in a whole brain exploration with a unified analytical framework. Here, we characterized dissociable cortical-cerebellar structural covariation patterns based on regional gray matter volume (GMV) across the brain in $n = 38{,}527$ UK Biobank participants. Our results invigorate previous observations in that important shares of cortical-cerebellar structural covariation are described as *1*) a dissociation between the higher-level cognitive system and lower-level sensorimotor system and *2*) an anticorrelation between the visual-attention system and advanced associative networks within the cerebellum. We also discovered a novel pattern of ipsilateral, rather than contralateral, cerebral-cerebellar associations. Furthermore, phenome-wide association assays revealed key phenotypes, including cognitive phenotypes, lifestyle, physical properties, and blood assays, associated with each decomposed covariation pattern, helping to understand their real-world implications. This systems neuroscience view paves the way for future studies to explore the implications of these structural covariations, potentially illuminating new pathways in our understanding of neurological and cognitive disorders.

NEW & NOTEWORTHY Cerebellum's association with the entire cerebral cortex has not been holistically studied in a unified way. Here, we conjointly characterize the population-level cortical-cerebellar structural covariation patterns leveraging ~40,000 UK Biobank participants whole brain structural scans and ~1,000 phenotypes. We revitalize the previous hypothesis of an anticorrelation between the visual-attention system and advanced associative networks within the cerebellum. We also discovered a novel ipsilateral cerebral-cerebellar associations. Phenome-wide association (PheWAS) revealed real-world implications of the structural covariation patterns.

cerebellum; cerebral cortex; phenome-wide associations (PheWAS); structural covariation

Correspondence: Z. Wang (zilong.wang@mail.mcgill.ca); D. Bzdok (danilobzdok@gmail.com).
Submitted 15 April 2024 / Revised 17 July 2024 / Accepted 18 July 2024

INTRODUCTION

Accumulating evidence suggested the cerebellum's role in various nonmotor and higher-order cognitive functions (1, 2). A series of tract-tracing studies in monkeys (3–8) and connectivity analyses using fMRI (9–12) identified multiple segregated, partially overlapping loops between different groups of neocortical and cerebellar regions, involving systems supporting both sensorimotor and many nonmotor cognitive function (13, 14). Here, we applied an alternative approach by quantitative modeling of the cortex-cerebellum structural covariation based on regional gray matter volume (GMV) that captures coherent population variation across thousands of people. This approach was naturally sensitive to systematic covariation relationships among multiple cerebrocerebellar regions, which were typically hard to investigate due to their parallel polysynaptic circuit links. This analytical approach traced out the patterns of which cerebellum subregions show structural variation that systematically co-occurs with structural variation in other brain network systems across individuals. To explore real-world relevance, we subsequently delineated the associations between these identified cortex-cerebellum structural covariation patterns (modes) and phenotypic measures indexing behavior, cognition, and physical conditions.

Invasive tract tracing studies provide a unique tool to isolate direct region-region axon pathways. The tract-tracing techniques are designed to meticulously study specific neural pathways in detail (15). However, this strict localizationist perspective treated the connections from a given brain region at hand as independent from those in other brain regions. Moreover, this technology, by its nature, is not applicable in humans (16). Furthermore, given the complexity of the brain and limited resources, it is challenging to conduct tract-tracing studies that cover larger territories of the brain (17, 18). In addition, between-species differences are another source of difficulty when extrapolating from cerebellum findings in animals to human biology.

Evolutionarily, as the association cortex (subserving executive control, language processing, and complex social interactions) disproportionately expanded in humans relative to monkeys and apes (19–22), parts of the cerebellar cortex (crus I/II) and cerebellar output dentate nucleus (ventrolateral proportion) have similarly enlarged disproportionately (23–26). Because the cerebral cortex and the cerebellum are highly interconnected, as the cerebral cortex expanded and evolved to become more functionally diverse in humans, it may be expected from the evolutionary perspective that the cerebellum expands and evolves in concert with the cerebral cortex to support those advanced cognitive functions (27). Despite the suspected evolutionary co-expansion between specific regions in the cortex and cerebellum, this "big" and "small" cortex of the human brain were routinely studied in isolation (23).

At the level of individual development, the postnatal cortical expansion pattern is known to show certain similarities to the evolutionary trajectory such that expanding higher associative cortical regions, supporting advanced cognitive functions, mature later in life. In contrast, primary visual, auditory, and sensorimotor regions appear already mostly mature at birth (22). Similarly, cognitive regions of the cerebellum myelinate and mature relatively later (crus I/II, VIIb, VIIIa) than the cerebellar regions involved in sensorimotor function (lobules I–IV, VIIIb, IX) (28, 29). This is consistent with the observation that the early matured regions support crucial survival functions at an early age, but the formation of advanced cognitive functions is subject to influences through environment and experience throughout life. The cerebellum is postulated to contribute its unique transform to sensorimotor, cognitive, and limbic functions (13, 14), so the coordinated maturation of the cerebellum and the cerebral cortex is crucial for the optimal development of cognitive and motor functions (30). However, previous studies typically investigated only the cerebral cortex (22) or only the cerebellar cortex (28) in isolation, without considering their interlocking relationships.

The evolutionary and developmental evidence provides support for the prediction that dedicated corresponding region sets across the entire cerebral cortex and cerebellum co-expand and co-mature jointly. If this is correct, it should be possible to observe coherent cerebellum-cortex resonance at the interindividual level too. In our present investigation, we hypothesized existence of one or more configurations of structural variation that simultaneously occur in a manner that is distributed spatially throughout the cortex-cerebellum complex. Our goal was to holistically chart the covariation between the entire cerebellar system and the entire cortical system at the population level with mission-tailored statistical tools.

Classic anatomical atlases (31, 32) view the cerebellum on the basis of structural landmarks via gross morphological features into the mediolateral division of vermis versus hemispheres, and the anterior lobe (lobules I–V), posterior lobe (lobules VI–IX), and flocculonodular lobe (lobule X). However, recent advances in functional neuroimaging analyses explored segmentation of the cerebellar cortex based on functional characteristics, such as patterns of neural activation being similar to other brain networks, or involvement in specific cognitive tasks or processes. In a group-averaged functional connectivity study opting for a winner-takes-all approach (WTA, each voxel is only assigned to a single brain system), Buckner et al. (9) discovered a roughly homotopic topographical mapping between the cortex and the cerebellum. This correspondence showed that larger higher-order cerebral networks are more extensively represented in the cerebellum. Furthermore, these authors found the majority of the human cerebellar cortex maps to some parts of the cerebral association cortex. The sensorimotor regions accounted for only a small portion of the cerebellum; with the notable exceptions of visual and auditory cortices. Ultimately, the cerebral association networks showed several anterior and posterior correlates in the cerebellum, mirroring the well-established dual representation of the body motor map (33–40). In the WTA approach, each cerebellar voxel is assigned to the most correlated brain network, supporting only one possibility for the cortical-cerebellar correspondence. This may have led to an incomplete view of the relationship between cerebral cortex and cerebellum. By embracing a latent-factor approach, we were able to explore the previously untapped possibility that each cerebellar subregion can be linked to several brain phenomena at the same time, and vice versa. Our approach thus

allowed for more than one explanation about the role of each subregion in the cerebellum in the context of the entire brain.

To achieve our goals, we mined the UK Biobank (UKBB) population cohort as it provides high-quality structural whole brain scans for ~40,000 individuals with ~1,000 in-depth phenotype measurements. By leveraging an analytical framework for doubly multivariate latent-factor decomposition, we here conjointly investigated the multiple concurrent GMV-based structural covariation patterns between the entire cerebellar cortex parcellated at 28 region resolution (with a structural and a novel functional atlas) and the entire cerebral cortex (at both the 7-functional-network and 100-subregion granularity) at the population level. We further profiled the key phenotypes associated with each decomposed covariation pattern (mode) to understand their real-world implications by means of phenome-wide association assays.

MATERIALS AND METHODS

Population Data Resource

The UK Biobank (UKBB) is an epidemiology resource that is unusually rich in behavioral and demographic assessments, medical and cognitive measures, and biological samples for ~500,000 participants recruited from across Great Britain (https://www.ukbiobank.ac.uk/). This openly accessible population data set aims to provide high-quality brain-imaging measurements for ~100,000 participants. The present study conducted under UK Biobank Application Number 25163 was based on the recent data release from February/March 2020 that augmented brain-scanning information and expert-curated image-derived phenotypes of gray matter morphology captured by T1-weighted structural MRI of 38,527 participants with 47% men, 53% women, and the ages of the participants were 40 to 70 yr when recruited (54.8 ± 7.5 yr). All participants provided written informed consent (for details see http://biobank.ctsu.ox.ac.uk/crystal/field.cgi?id=200).

Brain Imaging and Preprocessing Procedures

As an attempt to improve comparability and reproducibility, our study built on the uniform data preprocessing pipelines designed and carried out by FMRIB, Oxford University, Oxford, UK (41). Magnetic resonance imaging scanners (3-T Siemens Skyra) were matched at several dedicated data collection sites with the same acquisition protocols and standard Siemens 32-channel radiofrequency receiver head coils. The anonymity of the study participants was protected by defacing the brain scans and removing any identifying information. Automated processing and quality control pipelines were deployed (41, 42). Noise was filtered out by means of 190 sensitivity features to improve the homogeneity of the imaging data. This approach allowed for the reliable identification and exclusion of brain scans with artefacts, such as excessive head motion.

A three-dimensional (3-D) T1-weighted magnetization-prepared rapid gradient echo (MPRAGE) sequence at 1-mm isotropic resolution was used to obtain structural MRI brain-imaging data as high-resolution images of brain anatomy. Preprocessing included gradient distortion correction (GDC), skull-stripping using the Brain Extraction Tool (43), motion correction using FLIRT (44, 45), and nonlinear registration to MNI152 standard space at 1-mm resolution using FNIRT (46). All image transformations were estimated, combined, and applied by a single interpolation step to avoid unnecessary interpolation. Tissue-type segmentation into cerebrospinal fluid (CSF), gray matter (GM), and white matter (WM) was applied using FAST [FMRIB's Automated Segmentation Tool (47)] to generate full bias-field-corrected images. In turn, SIENAX (48) was used to derive volumetric measures normalized for head sizes.

Target Atlas Definitions

For the cerebral cortex, GM volume extraction was anatomically guided by the widely used Schaefer-Yeo reference atlas (49), yielding target features at 100- and 7-parcel resolutions: we extracted 100 cerebral cortical regions across the whole brain for each participant. We next normalized these raw cortical regional GM volumes to represent them as their ratios relative to the total cortical GM volume within each participant. In addition, at the 7-parcel resolution, we took their mean ratio to summarize all the cortical regions belonging to the same predefined canonical network, thus obtaining seven mean ratios for the seven networks for each participant. Finally, we z-scored the obtained quantities across participants for both the 100-region variable set and the 7-network variable set.

For the cerebellar cortex, we used two sets of target atlases to derive GM regional volumes for the sake of comparison: a widely used structurally defined atlas (50) based on macroanatomical landmarks and a recent functionally defined atlas (51) based on neural activity responses across many experimental tasks. This is to evaluate the functional cerebellar parcellation's effectiveness for explaining the structural covariation across individuals. The first set, sourced directly from the UK Biobank Imaging (UKBB data fields 25,893 to 25,920), is based on the structurally derived probabilistic SUIT atlas, which uses landmarks such as lobuli and vermis as a point of orientation (50). The structurally derived SUIT atlas divides the entire cerebellum into 28 neighbouring compartments, encompassing the left and right hemispheres of lobules I–IV, V, VI, crus I, crus II, VIIb, VIIIa, VIIIb, IX, and X, and the vermis of lobules V, VI, crus I, crus II, VIIb, VIIIa, VIIIb, IX, and X. The second set's GM volume extraction was informed by a novel functionally derived probabilistic parcellation of the entire cerebellum, which was based on an aggregate of seven extensive functional datasets (51). For the original version of the atlas, we generated a version with 28 interdigitated functional cerebellar regions (by fusing S2 and S3, as well as A3 and S5 on both the left and right side) to ensure similar number of atlas parcels and thus comparable statistical modeling properties between the two cerebellar atlases. In the end, mirroring the approach with the cortex, we calculated the regional ratios in relation to the total cerebellar GM volume and standardized them across participants for both the lobular anatomical atlas (50) as well as the functional atlas (52). A detailed description of different cerebellar regions and their functions can be found in Supplemental Table S1.

Building upon prior UK Biobank research (53, 54), we carried out a preliminary data cleaning step using standard linear regression. In particular, we removed the interindividual

variation in the aforementioned four groups of MRI-derived atlas region measures (i.e., *z*-scored ratio measures before the regression) that could be explained by the following nuisance variables of no interest: body mass index, head motion during task-related brain scans, head motion during task-unrelated brain scans, head position and receiver coil in the scanner (*x*, *y*, and *z*), position of scanner table, and the data acquisition site, in addition to age, age^2, sex, sex $\times$ age, and sex $\times$ age^2. The data cleaning was done by keeping the residuals orthogonal to all the nuisance variables from a linear projection of the *z*-scored ratio measures to the confounding space (55). Consequently, the *z*-scored, denoised regional ratio measures from 100 cortical regions, the mean ratio measures from the seven Schaefer-Yeo networks (49), and the ratio measures from 28 cerebellar regions—whether derived structurally or functionally—formed the foundation for subsequent analysis steps.

Population Covariation between Cerebellar Subregions and Cortical Regions

As the core analysis of our present investigation, we sought to investigate dominant patterns or "modes" of structural covariation that shed light on how structural variation among the cerebellar subregions can explain structural variation among all regions of the cortical brain mantle. Given the need to assess the multivariate relationship between two high-dimensional variable sets, partial least squares regression (PLSR) was our natural method of reference. A first variable set X was constructed from the cerebellar parcels (number of participants $\times$ 28 structurally or functionally derived cerebellar parcels matrix). A parallel variable set Y was constructed from the cortical subregional gray matter volume ratio or mean network gray matter volume ratio (number of participants $\times$ 100 whole brain cortical parcels matrix or 7 networks matrix).

$$X \epsilon R^{n \times p}$$

$$Y \epsilon R^{n \times q},$$

where n denotes the number of observations or UKBB participants, p is the number of cerebellar subregions, and q is the number of whole brain cortical subregions or cortical networks. Each column of the two data matrices was *z*-scored to zero mean (i.e., centering) and unit variance (i.e., rescaling) across the n participants.

This way, we had four input variable sets for PLSR and thus derived four dedicated PLSR models, each modeling a unique feature composition of cortical granularity and cerebellar modality of cortico-cerebellar covariation (Table 1).

The PLSR algorithm then addressed the problem of maximizing the covariance between the low-rank, mutually orthogonal projections from the two variable sets or data matrices. The two sets of linear combinations of the original variables are obtained by PLSR as follows:

$$T = XW \quad U = YC$$

$$t_l = Xw_l \quad u_l = Yc_l$$

$$cov(t_l, u_l) \propto t_l^T u_l, \text{ s.t.} cov(t_l, u_l) \text{ being maximized}$$

where orthonormal W and C indicate the respective contributions of X and Y, T and U denote the respective latent

Table 1. *Four combinations of cerebellar modalities and cortical parcellation granularity yielded four PLSR models*

Cerebellum	Cortex	
	100 Cortical Parcels	7 Cortical Networks
28 Functionally derived cerebellar parcels	Funct100region PLSR	Funct 7net PLSR
28 Structurally derived cerebellar parcels	Struct100region PLSR	Struct 7net PLSR

PLSR, partial least squares regression.

"modes" expression of joint variation based on the key patterns derived from X and from Y, t_l is the lth column of T, and u_l is the lth column of U. Note that for a given latent mode l, the overall signs of its weight vectors w_l and c_l are arbitrary, that is, overall positive and negative values can be flipped for a vector as a whole. We define modes as general principles of population variation in our target neural circuits that can be reliably extracted in brain structure at the population level. The goal of our PLSR approach was to find corresponding pairs of latent vectors t_l and u_l that yield maximal covariance in the derived latent embedding space. The data matrices X and Y were decomposed into L components iteratively, where L denotes the number of modes to be estimated by the model. Alternatively, PLSR finds the canonical vectors w_l and c_l that maximize the relationship between a linear combination of cerebellar volume ratio expressions (X) and a linear combination of brain volume ratio expressions (Y). By doing so, PLSR identifies the two concomitant projections Xw_l and Yc_l that optimized co-occurrence between patterns of whole cerebellum-cortex and whole cerebrum-cortex variation across participants.

Each identified mode was indicative of the principle cross-association between a constellation of within-subject cerebellar variations, and a constellation of within-subject cortical variations that occur in conjunction with each other at the population level. The set of L orthogonal modes are mutually uncorrelated by construction (56). They are also naturally ordered from the most important to the least important cortico-cerebellar covariation pattern based on the amount of variance explained between the latent cerebellar and cortical variable sets. Pearson's correlation between a pair of latent variables is commonly used to quantify the achieved degree of cross-correspondence between cerebellar subregions and cortical subregions or networks for a given mode. The first and strongest mode therefore explained the largest fraction of joint variational effects between combinations of cerebellar subregions and combinations of cortical regions. Each ensuing covariation mode captured a fraction of structural covariation that is not already explained by one of the $L - 1$ preceding modes. The variable sets were entered into PLSR after a confound-removal procedure based on previous UK Biobank research (cf. aforementioned).

Robustness of Derived Modes via Empirical Permutation Testing

To assess the solidity of each identified mode, we applied the identical analysis pipeline (as earlier) based on 1,000 permutation iterations (57). In each iteration i, we constructed

an empirical noise cerebellum variable set $\widetilde{X}_i = permute\ (X,\ axis = 1),\ i \in (1, \ldots, 1,000)$, by random permutation of the preprocessed cerebellar parcel measures within each participant, i.e., permuting each row of X. Once constructed, each permuted variable set $\widetilde{X}_i$ was fed into a PLSR model with the unpermuted, original cortical features (variable set Y) and decomposed into L hypothetical cortex-cerebellum covariation modes composed of L pairs of latent column vectors $\widetilde{t}_{i,l}, \widetilde{u}_{i,l}$ (as earlier). The explanatory power corr(t_l, u_l) of each of our actual modes of PLSR models was then compared with the hypothetical mode $\widetilde{l_{max}} = \underset{l}{argmax}\left(\frac{\sum_{i=1}^{1,000}\mathrm{corr}\left(\tilde{t}_{i,l},\tilde{u}_{i,l}\right)}{1,000}\right)$ whose explanatory power was on average the highest across 1,000 permutation iterations. In other words, the 1,000 explanatory power values of $\widetilde{l_{max}}$ yielded a null distribution of the expected highest explanatory power for our actual modes (58). We kept only the actual modes l whose P value $P_l = \frac{\sum_i\left[\mathrm{corr}(t_l,u_l)<\mathrm{corr}\left(\tilde{t}_{i,\widetilde{l_{max}}},\tilde{u}_{i,\widetilde{l_{max}}}\right)\right]}{1,000} < 0.001$. This permutation analysis scheme intentionally aimed to break the link between homologous cortex-cerebellum pairs within individuals to generate an empirical null distribution. These noise data simulations allowed testing of the robustness of covariation patterns in the hypothetical population.

Phenome-Wide Profiling

To enrich our core analysis (cf. aforementioned), we aimed to interrogate the practical implications of the derived cortico-cerebellar covariation modes. We sought to understand their links to UK Biobank traits across a deliberately broad spectrum of predefined phenotype and categories. To that end, we performed an in-depth annotation of the cortico-cerebellar modes by screening 977 phenotypes encompassing lifestyle factors, cognitive tests, and physical health assessments. To carry out this phenome-wide association analysis (PheWAS), we sourced phenotypic features through two specialized tools tailored for aggregating, cleaning, and normalizing UK Biobank phenotype data according to predefined rules. We started with a raw collection of ~15,000 phenotypes that were fed into the FMRIB UK Biobank Normalisation, Parsing And Cleaning Kit (FUNPACK v.2.5.0; https://zenodo.org/record/4762700#.YQrpui2caJ8). Through FUNPACK, we curated and harmonized the data, focusing on a collection of phenotypes linked to 11 categories of interest. The results from FUNPACK, which yielded ~3,300 phenotypes, were then fed into PHEnome Scan ANalysis Tool (59) (PHESANT, https://github.com/MRCIEU/PHESANT) for further refinement, cleaning, and data categorization. The resulting final set of 977 phenotypes of interest derived from PHESANT was subsequently analyzed against discovered covariation modes to probe for associations between cortico-cerebellar structural covariation pattern expressions and target phenotypes.

To be specific, we used FUNPACK on the UKBB sample to extract phenotype information covering 11 major categories, including "blood assays," "cognitive phenotypes," "early life factors," "lifestyle and environment—alcohol", "lifestyle and environment—exercise and work," "lifestyle and environment—general," "lifestyle and environment—tobacco," "mental health self-report," "physical measures—bone density and sizes," "physical measures—cardiac & blood vessels," and "physical measures—general." These categories of interest were predefined in the FUNPACK utility (-cfg fmrib arguments) and they excluded any brain-imaging-derived information. As there were only four phenotypes associated with diet, we excluded this category from downstream analysis. The FUNPACK setting defining the phenotype categories contained a built-in toolkit tailored to the UKBB which we used to refine the phenotype data, such as removing "do not know" responses and replacing unasked dependent data. For example, a participant who answered that they do not use mobile phones was not asked how long per week they spent using a mobile phone. Here, FUNPACK would fill in a value of zero hours per week as a response. As such, FUNPACK's built-in rule-based pipeline yielded 3,330 high-quality phenotype columns.

The intermediate output from FUNPACK was then fed into PHESANT, which is an established tool for further curating UK Biobank phenotypes. In addition to combining phenotypes across visits, data cleaning, and normalization, PHESANT categorized the data as belonging to one of four data types: categorical ordered, categorical unordered, binary, or numerical. All categorical unordered columns were one-hot encoded into binary columns to represent a single response. For example, the employment status phenotype was originally encoded as a set of categorical indicators representing different contexts (e.g., retired, employed, on disability). These conditions were converted into a binary column (e.g., retired true or false). We then combined the output of categorical one-hot encoding of unordered phenotypes with all measures classified by PHESANT as binary, numerical, or categorical ordered. In so doing, the final set comprised 977 phenotypes.

We deployed both FUNPACK and PHESANT with their default parameter choices. As a result, all columns containing fewer than 500 participants were automatically discarded from further analysis according to PHESANT's default protocol. Moreover, FUNPACK by default assessed pairwise correlation between phenotypes and kept only one phenotype of a set of highly correlated phenotypes (>0.99 Pearson's correlation ρ). For example, left and right leg fat percentages were highly correlated (Pearson's $r = 0.992$). Hence, only right leg fat percentage was included in the final set of phenotypes. The choices of which phenotypes to discard were also automatically streamlined and conducted by FUNPACK.

We then explored and charted the relationships between the subject-wise expression of specific cortico-cerebellar covariation patterns, with their single-subject expression, and the portfolio of 977 phenotypes, ensuring appropriate correction for multiple comparisons. By computing the Pearson correlation between each phenotype and the interindividual variation in the cortical latent variable and cerebellar latent variable respectively, we discerned both the association strength and the accompanying statistical significance of their relationship. For each identified covariation pattern, we applied two widely established corrections for multiple comparisons to account for the numerous association tests being evaluated in our assay. We first used Bonferroni's correction, adjusting based on the number of phenotypes tested (0.05/977 = 5.11*e*-5). In addition, we examined the significance of

our correlation strength through the false discovery rate (FDR), another widely accepted method for multiple comparison correction that is more lenient than Bonferroni's approach. The false discovery rate (60) was set as 5% (42, 61, 62) and computed for each covariation mode following standard practice (63). To aid in visualization, all phenotype results were color-coded and organized based on category membership as per definitions provided by FUNPACK.

RESULTS

Previous neuroscience studies have rarely directly investigated the GMV-based covariation between the entire cerebral cortex and the entire cerebellum in humans (22, 23, 28), let alone across a large cohort of subjects. Our central analysis yielded different numbers of statistically significant derived latent modes: two modes for "Funct 7network," six modes for "Funct 100region," four modes for "Struct 7network," and seven modes for "Struct 100region" (Table 1). Here, we first attend to the selected cortical and cerebellar structural variation weights (*U* and *V*, representing the respective contributions of cortical and cerebellar subregions to the derived latent modes, cf. MATERIALS AND METHODS). We then present the significant phenotype profiles associated with cortical latent variable and cerebellar latent variable.

Dissociation between Higher and Lower Neural System in Cortex-Cerebellum Covariation

Across examined models (Table 1), the most explanatory and robust sources of population variation revealed a highly consistent higher-level cognitive system and the low-level visual-sensorimotor system interplay in the cortex-cerebellum covariation, no matter which atlas parcellation definition was used. We start with the model "Funct 7net."

Mode 1 exhibited the highest explanatory power of 0.41, and juxtaposed a sensorimotor-visual network against higher-order cognitive networks, as manifested by the opposing directions of structural variation trends. As can be seen for the cerebellum (Fig. 1), we observed the positive weights in regions D2 distributed around the border between lateral lobule VI and crus I, between lateral crus II and lobule VIIb, and scattered in lobule IX; generally known to be associated with executive functions (52, 64). Central and lateral crus I, crus II, and paravermal IX, related to the fused social-language regions S2 and S3, also exhibited strong variation weights. The motor associative atlas region M2 related to the mouth at the intersections of bilateral paravermal lobules VIIb and VIIIa showed positive variation weights, too. For the cerebral cortex, we observed structural variation in the executive-control network (ECN), default mode network (DMN), limbic network, and salience/ventral attention network

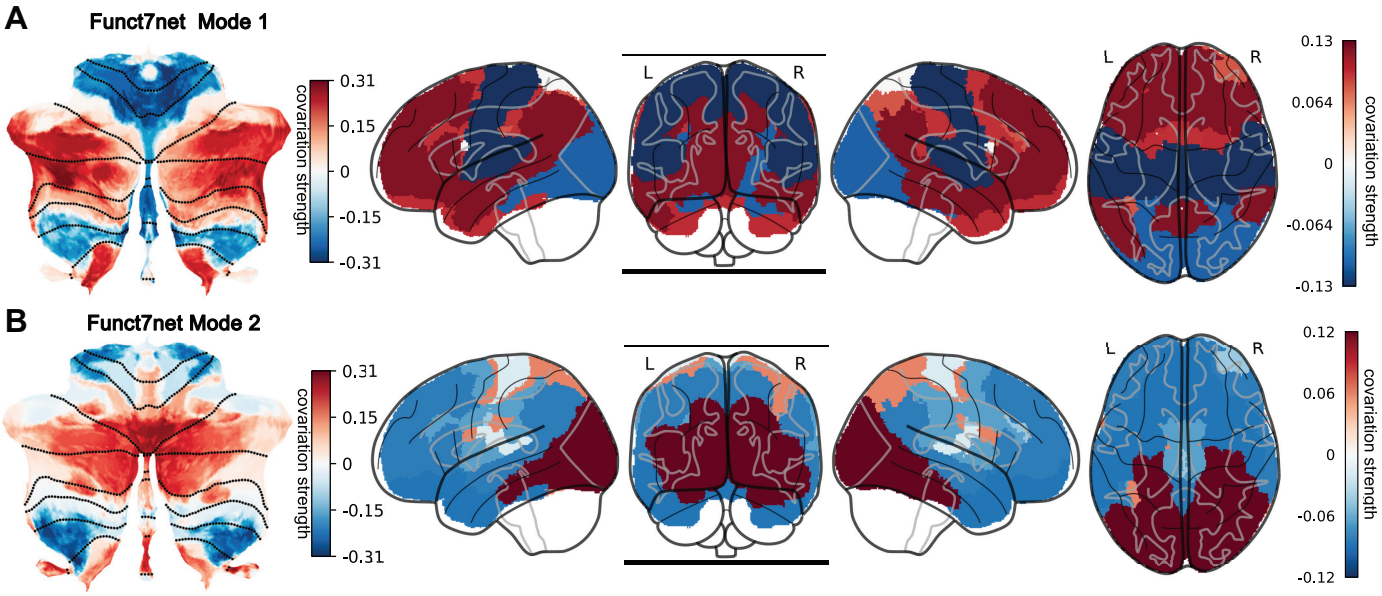

Figure 1. Funct7net *modes 1* and *2* explained contrasting gray matter volume (GMV)-based variation in the higher cognitive-lower visuosensorimotor system interplay vs. exogenous visuoattentional-endogenous cognitive system. *Mode 1* and *mode 2* in cerebellar functional parcellation with cortical 7 network averaged ('Funct 7net') displayed a clear contrast between higher cognitive system and lower visual-somatosensory system. *A*: *mode 1* had an explanatory power of 0.41. One end of structural variation weights was found in regions associated with executive functions and social-language processing in the cerebellum and general higher-order cognitive networks in the cerebral cortex. The opposite end of structural variation weights was observed in other cerebellar regions and the sensorimotor and visual networks in the cerebral cortex. Weak weights were assigned to the dorsal attention network (DAN). The cortical variation patterns align with the DMN-visuomotor distinction, whereas the cerebellar variation patterns correspond to the classical double motor representation and the triple nonmotor representation. *B*: *mode 2* had an explanatory power of 0.28. One end of structural variation weights was observed in bilateral eye atlas regions in the cerebellum, as well as in executive-function and social-language regions. The cerebral cortex exhibited strong variation weights in the visual network and lesser variation weights in the DAN. The opposite end of structural variation weights was found in specific cerebellar regions associated with introspection, action observation, and lower limb functions, which showed structural covariation with other higher-order cognitive networks in the cerebral cortex. Notably, an antagonist relationship observed between the DAN and other higher-order cognitive networks was potentially anchored in the cerebellum. Red, blue, and white indicate positive, negative, and zero weights that maximize the covariance between cortical and cerebellar latent variables. DMN, default mode network.

(VSN) (Fig. 1*A* and Supplemental Fig. S1*A*). Together, higher-order cognitive function-related regions in both the cerebellum and cortex showed the same direction of structural variation.

Conversely, in *mode 1*, sensorimotor and action-related regions of both the cerebellum and the cortex exhibited a structural covariation pattern that was directionally opposite to that observed in the higher-order cognitive regions. For the cerebellum, we observed the strongest negative weights in the upper limbs atlas regions M3 that were defined by a significant proportion of lateral lobules I–V and VIIIb and complex action atlas regions A1 that sit across lobules I–V vermis and extended into lobule VI and further extended from crus II to lobule VIIIb vermis. In addition, we observed weaker weights in action observation atlas regions A2 sitting on the border between lateral lobules V and VI, between lobules VIIIa and VIIIb, and lower limbs atlas regions M4 occupying lateral lobules I–V and VIIIb regions in the cerebellum. Finally, we observed the weakest variation weights in the oculomotor vermis M1 (52), which was mostly located in VI vermis, and some portions of lobule IX/X vermis. For the cerebral cortex side of this population mode, we obtained strong contribution in the sensorimotor network and visual network (Fig. 1*A* and Supplemental Fig. S1*A*). The cortical weights in *mode 1* were broadly consistent with the DMN-visuomotor divergence of neural systems described by Margulies et al. (65) and, before, by Mesulam (66) such that the DMN and the unimodal visual, sensorimotor networks' weights were at the two extreme ends while other higher-order cognitive networks were situated in between. The cerebellar weights in *mode 1* were also highly consistent with the most dominant functional gradient in the cerebellum (67) and with the classical double motor representation (lobules I–VI and VIII) and the recently proposed triple nonmotor representation (lobules VI/crus I, crus II/VIIb, and IX/X) (9, 12).

Mode 2 showed the second-highest explanatory power of 0.28 in our analyses based on the functionally derived cerebellum atlas. *Mode 2* separated a visual-attention network from other functional networks that were assigned opposite to structural covariation weights. In the cerebellum, we observed one extreme pole of structural variation weights in M1 (cf. aforementioned). Executive-function region D1 also exhibited strong implications in *mode 2*. This region consisted of two patches on the cerebellar cortex at the border between central lobule VI and crus I, and between central crus II and VIIb. It also stretched along paravermal lobules VI, crus I, and crus II. We further observed relevant positive weights in two social-language atlas regions: S1 defined by extensive coverage of paravermal crus I, crus II, and areas into lobule VI, VIIb, and S2_3 (cf. aforementioned). For the cerebral cortex, we observed the most prominent structural variation weights in the visual network and some implications of the dorsal attention network (DAN) (Fig. 1*B* and Supplemental Fig. S1*B*).

The opposite direction of structural variation in *mode 2* was found in lateral lobule VIIIb and IX, in the fused regions A3 and S5, related to introspection and action observation (52). We further observed significant structural variation weights in lower limbs regions M4 and action observation region A2 (cf. aforementioned). These cerebellar regions showed systematic structural covariation with default mode network (DMN), limbic network, VSN, and executive control network (ECN) in the cerebral cortex (Fig. 1*B* and Supplemental Fig. S1*B*). Notably, our findings witness an antagonist relationship between DAN and other higher-order neural systems here modeled as anchored in the cerebellum, which was less recognized than their established anticorrelation relationship in the cortex (68–71).

100-region Cortical Parcellation Mirrors the Dissociation in 7-Network Cortical Atlas

Our second model used cerebellar functional parcellation with cortical 100-region parcellation ("Funct 100region," Table 1) that is based on the same cortical atlas but differed from the "Funct 7net" model (cf. aforementioned) by higher resolution. The left and right homologous regions in 100-region parcellation are also separated, whereas in the 7-network parcellation there is no left-right hemispheric distinction. Our "Funct 100region" model broadly reiterated the trend of motor versus cognitive systems detailed in *mode 1* (explanatory power 0.49, Fig. 2*A* and Supplemental Fig. S2*A*) and visuoattention network's anticorrelation with other network systems in *mode 2* (explanatory power 0.32, Fig. 2*B* and Supplemental Fig. S2*B*) with the more granular cortical subregional specification. The cerebellar weights in each pair of *mode 1* and *mode 2* of "Funct 100region" and "Funct 7net" were quite similar, with *mode 1* absolute Pearson's $|r| = 0.99$, P value $<10^{-29}$ and *mode 2* absolute Pearson's $|r| = 0.98$, P value $<10^{-19}$, after correlating across respective cerebellar region weights of the two cerebellum-brain covariation model instances.

Although the pattern of cerebellar weights was extremely similar, the "Funct 100region" solutions provided a more fine-grained analysis of the cortical patterns than the "Funct 7net" solution—showing that the structural covariation concentrates on certain subsets of regions within each network rather than on the entire network. For *mode 1*, one end of the structural variation weights was concentrated in bilateral temporo-occipital cortex including left visual word form area, left middle-inferior temporal gyrus, left temporal pole, right middle-inferior temporal gyrus, and right fusiform gyrus. On the other end of structural variation were bilateral parieto-occipital lobes including primary visual cortex, extrastriate cortex, retrosplenial cortex, lingual gyrus, primary sensorimotor cortex, premotor cortex, and surprisingly primary auditory cortex (Fig. 2*A* and Supplemental Fig. S2*A*). In *mode 2*, we observed one extreme end of structural variation weights in bilateral parieto-occipital lobes including primary visual cortex, extrastriate cortex, fusiform gyrus, intraparietal sulcus (IPS) and cuneus, retrosplenial cortex, and precuneus, and the other end of structural variation weights in bilateral frontal cortex and anterior temporal lobe, including the temporal pole, parahippocampal gyrus, orbitofrontal cortex, ventrolateral prefrontal cortex and anterior insula cortex, cingulate cortex, and dorsolateral prefrontal cortex (Fig. 2*B* and Supplemental Fig. S2*B*).

An Ipsilateral Axis of Cortical-Cerebellar Variation

Despite the known mainly contralateral fiber connection between the cerebellum and the cerebral cortex, we persistently observed an ipsilateral pattern in the 100-region

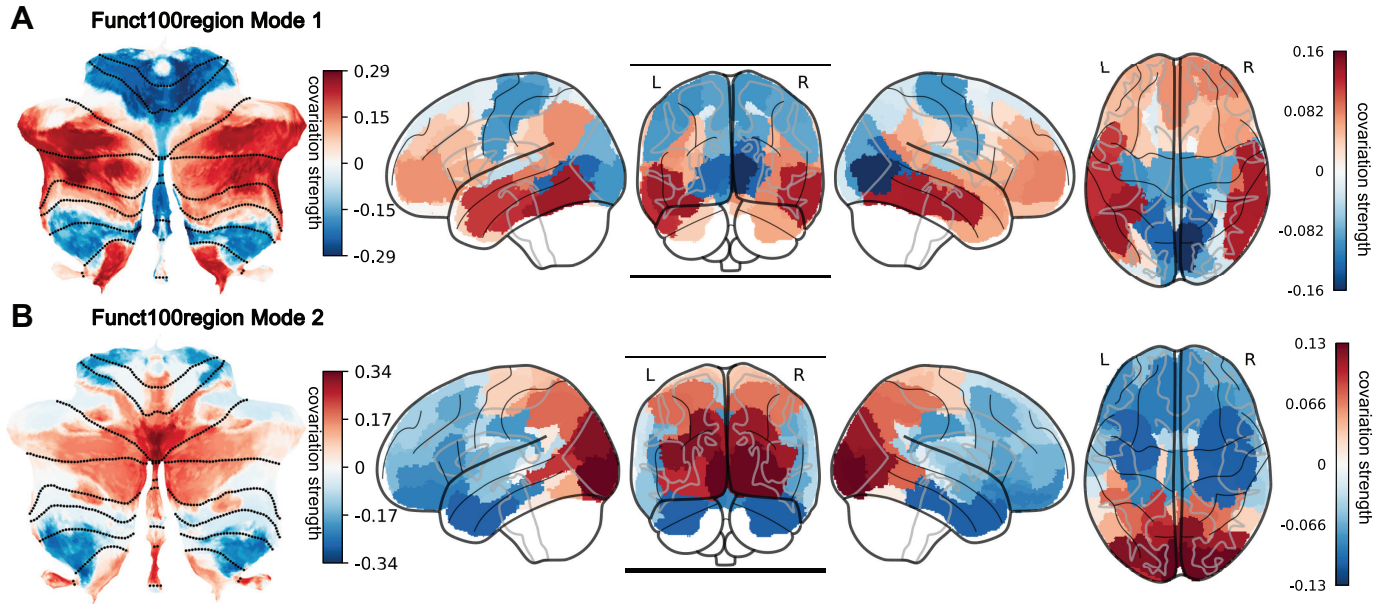

Figure 2. Funct100region *mode 1* explains opposite gray matter volume (GMV)-based variation in primary visual/sensorimotor regions vs. higher associative regions, whereas *mode 2* explains visual-attentional regions to anticorrelate with higher associative regions. *Mode 1* and *mode 2* in cerebellar functional parcellation with cortical 100 region parcellation ("Funct 100region") broadly reiterate the patterns observed in the first two modes of "Funct 7net," with almost perfectly correlated cerebellar weights respectively (*mode 1*: $r = 0.99$, P value $<10^{-29}$; *mode 2*: $r = 0.98$, P value $<10^{-19}$). As cortical weights were more different, here we only describe the differences in cortical weights. For the description of cerebellar weights, see Fig. 1. *A*: *mode 1* had an explanatory power of 0.49. One end of structural variation weights was concentrated in the bilateral temporo-occipital cortex. The opposite end of structural variation weights was distributed in bilateral parieto-occipital lobes and the primary somatosensory cortex. *B*: *mode 2* had an explanatory power of 0.32. One end of structural variation weights was observed in bilateral parieto-occipital lobes. The opposite end of structural variation weights was found in bilateral frontal cortex and anterior temporal lobe.

cortical parcellations such that the dominating regions in the cerebellum and cerebral cortex variation share the same end of weights for a given side of the brain.

Mode 3 ("Funct 100region") showed an explanatory power of 0.30 (Fig. 3 and Supplemental Fig. S2*C*). Notably, the entire left and right cerebellum showed opposite variation trends. In the left cerebellum, we observed the most significant structural variation concentrated in regions centering on the posterior lobule VI, lateral anterior crus I, lateral VIIb, anterior VIIIa, lobule IX/X, and vermal I–VI that are associated with executive function (working memory) as per atlas, areas of paravermal crus I, crus II, and areas extending into lobule VI, VIIb that are related to social-language and the intersections of bilateral paravermal lobules VIIb and VIIIa related to mouth in the left cerebellum. In this mode's counterpart in the cortex, left cortical regions varied in the same direction as the left cerebellum, especially the primary auditory cortex, Broca's area, lower primary sensorimotor regions, and inferior frontal gyrus. On the contrary, the right cerebellum varied in the same direction as right cortical regions, especially the right cerebellar regions associated with executive function, social-language, motor and complex action; right cortical regions, such as inferior/middle temporal gyrus, fusiform gyrus, temporoparietal junction

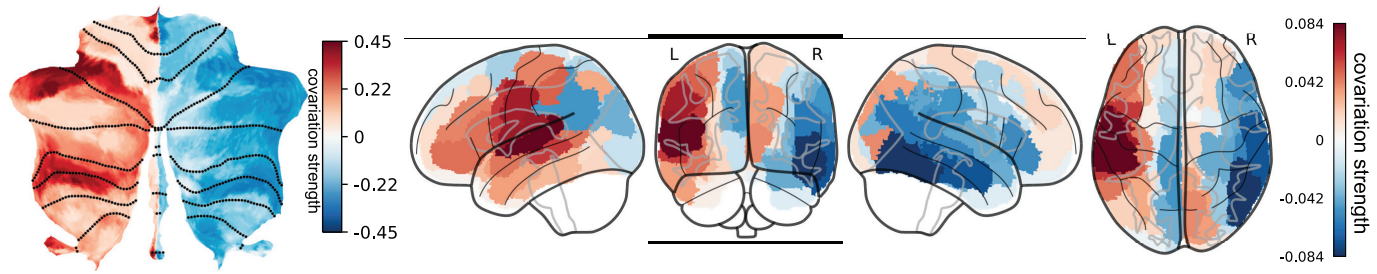

Figure 3. Driving ipsilateral principles in cerebellum-cortex correspondence as a key feature of population brain gray matter volume (GMV)-based variation. An ipsilateral pattern for the dominating weights' direction in the cerebellum and cerebral cortex appeared in "Funct 100region" *mode 3*. "Funct 100region" *mode 3* had an explanatory power of 0.30. The entire left cerebellum and right cerebellum showed completely opposite directions of structural variation weights. One end of structural variation weights concentrated in specific regions associated with executive function, social-language, and motor functions in the left cerebellum, and in the left cerebral hemisphere including the primary auditory cortex, Broca's area, and inferior frontal gyrus. Conversely, the other end of structural variation weights observed in right cerebellar regions roughly symmetric to the left side, associated with executive function, social-language, and motor functions, and in the right cerebral hemisphere including inferior/middle temporal gyrus, fusiform gyrus, temporoparietal junction (TPJ), and primary auditory cortex. The precuneus and posterior cingulate cortex exhibited a contralateral pattern.

(TPJ), and primary auditory cortex. Interestingly, the cortical regions conforming to the usual contralateral patterns were the precuneus and posterior cingulate cortex, albeit with less significant weights. Together, *mode 3* ("Funct 100region") displayed a robust ipsilateral pattern such that either side of cerebellum varied in the same direction as the dominant cortical regions on the same side of the brain.

The ipsilateral cerebellar-cortical pattern was also observed in a mode based on the structural atlas: mode 2 ("Struct 100region"; Supplemental Fig. S4*A* and Fig. S8*A*) that had an explanatory power of 0.29, on par with *mode 3* ("Funct 100region"). One end of the most prominent structural variation weights was seen in right crus I, crus II, and left lobule VIIIa/b, and in the right superior temporal sulcus, auditory cortex, somatosensory cortex, TPJ, and dorsolateral prefrontal cortex (dlPFC); the other end of the most significant structural variation weights were seen in left crus I, crus II, and right lobule VIIIa, and in the left temporal lobe, fusiform gyrus, supramarginal gyrus, angular gyrus, and some visual/auditory/motor-associative areas. Again, the only cortical regions conforming to the usual contralateral patterns were the precuneus and posterior cingulate cortex.

Comparing the cerebellar weights in modes derived from the functional versus structural cerebellum atlas, the cerebellar weights in the former were more homogeneous for either side such that all the cerebellar regions on the left show the opposite direction of structural variation to all the cerebellar regions on the right, whereas the latter showed both directions of structural variation on each side. Comparing *mode 3* ("Funct100region") and *mode 2* ("Struct100region"), we found that the cortical weights were highly similar (Pearson's $r = -0.82$, P value $<10^{-25}$). Thus, this suggests that the modes from the functionally and structurally derived cerebellar atlas point to at least some overlapping associative brain findings. Overall, the strongest weights still followed the ipsilateral pattern.

Anatomical Cerebellar Regions Capture Less Structural Variation

We focused our results on the functionally derived cerebellum atlas because the explanatory power of *mode 1*, *mode 2*, *mode 3*, and *mode 4* from the structurally derived cerebellum atlas were 0.20, 0.19, 0.13, and 0.12 respectively, achieving only about half the explanatory power of those from the functionally derived cerebellum atlas. This observation suggested that the functionally derived cerebellum atlas explained the data better. We also found these modes were harder to interpret, especially regarding the cerebellar latent variables. But these cerebellar patterns arguably reconciled with several classical cerebellar functional organizations, such as crus I/II's crucial role in DMN and attention, lobule I–IV/VIII's role in motor function, and vermis or flocculonodular lobe's role in limbic function (2, 72).

Struct 7net's *mode 1* (Supplemental Fig. S3*A* and Fig. S7*A*) and *mode 4* (Supplemental Fig. S3*D* and Fig. S7*D*) generally reproduced a similar pattern to those of "Funct 7net" *mode 1*'s (Fig. 1*A* and Supplemental Fig. S1*A*) cortical weights after correlating across respective cortical regions, with *mode 1* absolute Pearson's $|r| = 0.94$, P value $<10^{-47}$ and *mode 4* absolute Pearson's $|r| = 0.92$, P value $<10^{-42}$. In *mode 2* (Supplemental Fig. S3*B* and Fig. S7*B*) of "Struct 7net," we captured a strong reciprocal relationship between DAN and DMN/limbic network that was highlighted in *mode 2* of "Funct 7net" (Fig. 1*B* and Supplemental Fig. S1*B*), which added more evidence that an antagonist relationship between DAN and DMN could be anchored in the cerebellum. In *mode 3* of "Struct 7net" (Supplemental Fig. S3*C* and Fig. S7*C*), we observed a similar anticorrelation between ECN-DAN and DMN-limbic system. For *mode 1*, the cerebellar regions varying concurrently with the higher-order cognitive networks except DAN were bilateral crus I/II and lobule X, whereas the cerebellar regions consistent with sensorimotor network were lobules VIIIa/b, lobules IX, and anterior lobe to a lesser extent. This pattern roughly forms a double-motor (lobules I–VI, VIII, and additionally IX), triple-nonmotor representation (lobules crus I, crus II, and X) in the cerebellum (12). For *mode 2*, the cerebellar regions tied with DMN and limbic networks were anterior lobe, vermis across the posterior lobe, bilateral lobules VIIIb and lobule X, whereas the cerebellar regions coherent with DAN were bilateral lobules VII. For *mode 3*, the cerebellar regions covarying with the ECN and DAN were lobule X vermis, anterior lobe, bilateral lobules VIIIb and IX, and crus I, whereas the cerebellar regions covarying with DMN and limbic system were bilateral lobules VIIb, crus II, and lobules VIIIa. For *mode 4*, the cerebellar regions coherent with the higher-order cognitive networks except limbic network were the posterior lobe up to crus II, excluding most of the cerebellar vermis or lobule X, whereas the cerebellar regions consistent with visual-motor networks were the anterior lobe plus crus I to a lesser extent, which reminded us of the classical anterior motor—posterior cognitive cerebellum segmentation (14, 73–77).

Finally, *mode 3* (Supplemental Fig. S4*B* and Fig. S8*B*) in our structurally derived cerebellum atlas with cortical 100 region parcellation ("Struct 100region") corresponded to "Funct 100region" *mode 1* (Fig. 2*A* and Supplemental Fig. S2*A*), and their cortical weights were highly correlated with absolute Pearson's $|r| = 0.85$, P values $<10^{-27}$. It also corresponded to "Struct 7net" *mode 1* (Supplemental Fig. S3*A* and Fig. S7*A*), with highly correlated cerebellar weights reaching absolute Pearson's $|r| = 0.93$, P values $<10^{-11}$. *Mode 5* (Supplemental Fig. S4*C* and Fig. S8*C*) corresponded to "Funct 100region" *mode 2* (Fig. 2*B* and Supplemental Fig. S2*B*) and "Struct 7net" *mode 2* (Supplemental Fig. S3*B* and Fig. S7*B*), with an explanatory power of 0.21. The cerebellar weights between *mode 5* and "Struct 7net" *mode 2* were highly correlated with Pearson's $r = 0.84$, P values $<10^{-7}$. However, the cortical weights were very different from "Funct 100region" *mode 2*. We observed the frontal eye field and IPS that are key regions of the DAN dominated one end of variation, whereas retrosplenial cortex (RSC), insular cortex, auditory cortex, and inferior prefrontal cortex, which play important roles for episodic memory, limbic function, and linguistic function dominated the other end. This pattern overall corresponded with the DAN versus DMN-limbic contrast seen in Struct7net *mode 2*'s cortical weights. The explanatory powers of 0.27 and 0.21 were still much less than the explanatory power of "Funct100region" *mode 1* and *2*, which reaffirmed our focus on the analysis of functionally derived cerebellum atlas.

Funct7net *Mode 1* Shows Phenotypic Signature with Distinct Arrays of Cognitive, Lifestyle, Physical Conditions, and Blood Traits

To understand relevant real-world implications of the derived cerebellar-cortical variation modes, we carried out phenome-wide association assays (PheWAS): we tested links of 977 phenotype measurements across all the subjects with cerebrocerebellar *modes 1* and *2* from Funct 7net (Figs. 4 and 5) and Funct 100region PLSR results (Supplemental Figs. S5 and S6). This revealed the unique phenotypic profiles of each mode and provided a wealth of potentially undiscovered brain-phenotype connections. We paid special attention to the phenotypes whose association with either latent variable was above the Bonferroni correction thresholds.

In *mode 1* (Funct7net; Fig. 4), where the higher cognitive-lower sensorimotor system interplay explained the most cerebello-cortical covariance, overall, there appeared to be a closer link between complex cognitive ability, obesity, the likelihood of cardiovascular diseases, a sedentary lifestyle, and the cortical latent variable. In addition, psychomotor processing speed, physical activity, and angiogenesis were better associated with cerebellar latent variable.

The association between many cognitive phenotypes and the latent cortical and cerebellar variables surpassed other phenotype categories by a margin. Generally, most of the significant cognitive phenotypes are common to both the cortex and the cerebellum. Yet, they showed more dominant associations with the cortex component than with the cerebellum component of our *mode 1*, including mostly fluid intelligence tests, alphanumeric trail-making tests (TMT-B), initial answer for prospective memory, and matrix completion tasks that require abstract reasoning, complex executive functions, focused visual attention, and motor control (78–80). The phenotypes that showed equivalent or even stronger associations with the cerebellum are digit symbol substitution test (DSST) (81), reaction time test, and numeric trail-making test (TMT-A), a widespread hand-eye coordination test, which measures the psychomotor speed and overall efficiency of operations and are known to be closely related to the cerebellum, as evidenced in previous studies (1, 82–84). Nonetheless, both the cerebellar and cortical

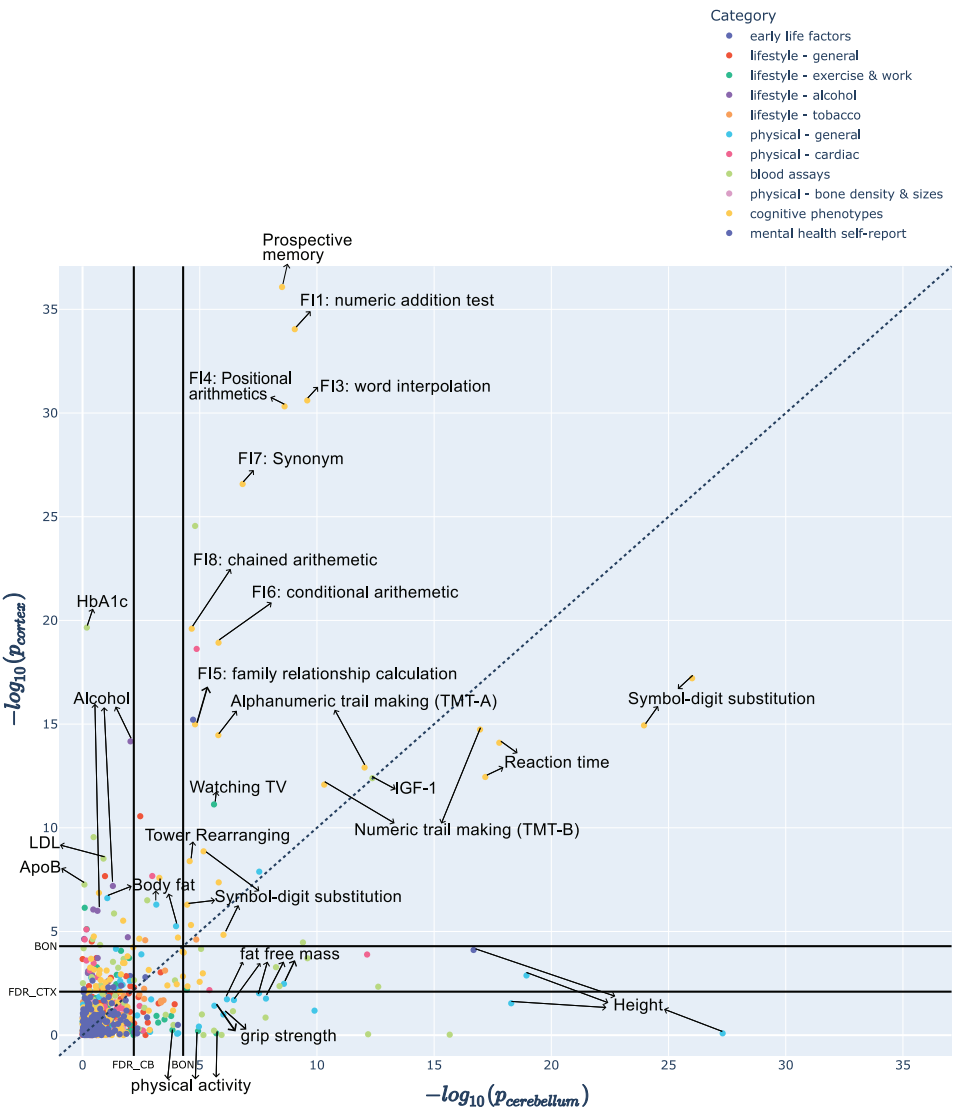

Figure 4. Funct 7net *mode 1* shows phenotypic signature with distinct arrays of cognitive, lifestyle, physical conditions, and blood traits for the higher-lower system correspondence across the cortex and cerebellum. *Mode 1* (Funct7net) cerebellar-cortical phenotype profiles. The *x*-axis shows the −log_10 (*P* value) of the cerebellum whereas the *y*-axis shows the −log_10(*P* value) of the cortex. The *P* values came from the Pearson's correlation between the cortical mode or the cerebellar mode and the phenotypes. Top 50 phenotypes for Funct7net *mode 1* (Supplemental Table S2) list the actual Pearson's correlation strength for the top 50 phenotypes. The Bonferroni correction threshold (BON) and false discovery rate (FDR) are plotted for the cortex and the cerebellum on the respective axis. Phenotypes near the upper-left part of the figure are more strongly associated with the cortex while those near the lower-right corner are more strongly associated with the cerebellum. The phenotypes near the diagonal are relevant for both the cortex and the cerebellum. The phenotypes at the lower-left corner bordered by the two BON threshold lines are considered insignificant.

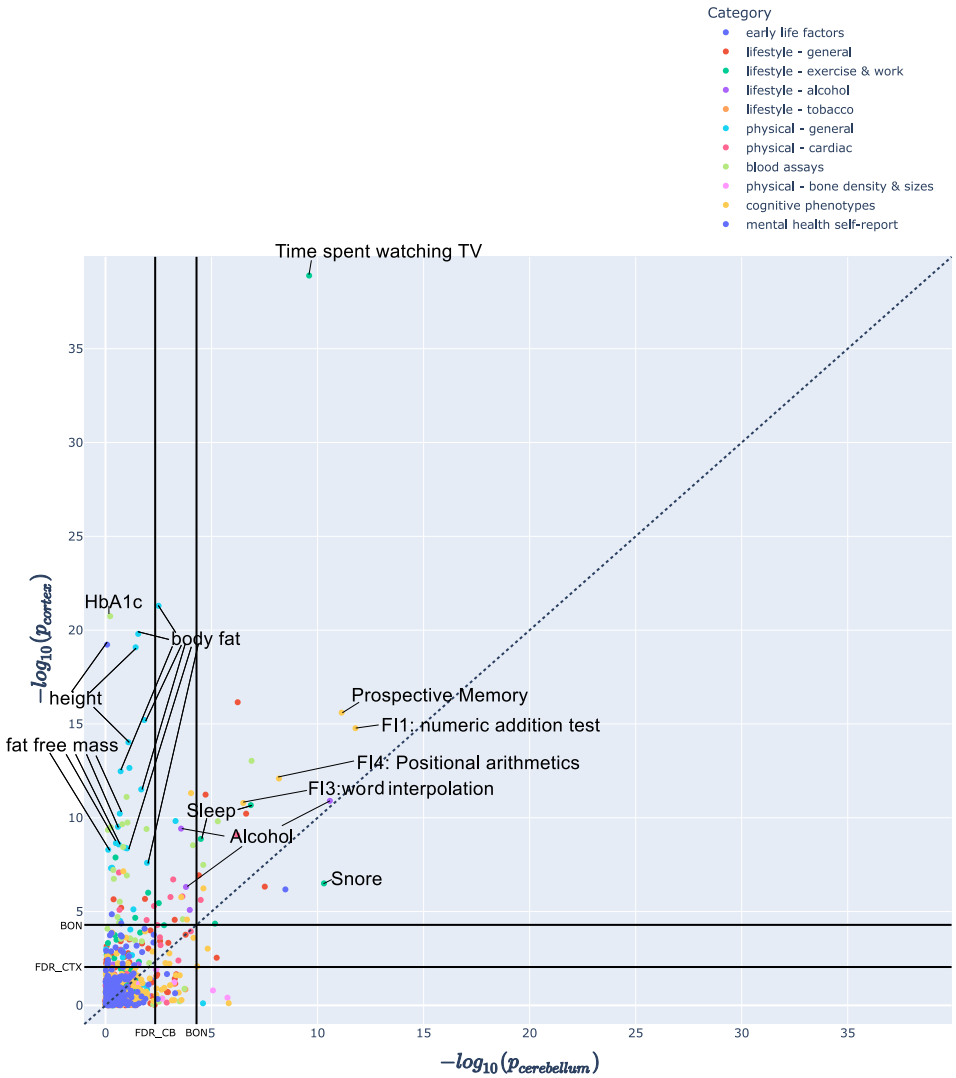

Figure 5. Funct7net *mode 2*'s phenotype array is driven by time spent watching TV. Most phenotypes show more unique associations with the cortex than the cerebellum, but cognitive phenotypes for fluid intelligence and executive function are significant for the cortex and the cerebellum. The *x*-axis shows the −log_10(*P* value) of the cerebellum whereas the *y*-axis shows the −log_10(*P* value) of the cortex. The *P* values came from the Pearson's correlation between the cortical mode or the cerebellar mode and the phenotypes. Top 50 phenotypes for Funct7net *mode 2* (Supplemental Table S3) list the actual Pearson's correlation strength for the top 50 phenotypes. The Bonferroni correction threshold (BON) and false discovery rate are plotted for the cortex and the cerebellum on the respective axis. Phenotypes near the upper-left part of the figure are more strongly associated with the cortex while those near the lower-right corner are more strongly associated with the cerebellum. The phenotypes near the diagonal are relevant for both the cortex and the cerebellum. The phenotypes at the lower-left corner bordered by the two BON threshold lines are considered insignificant.

mode 1 (Funct7net) showed robust associations with a number of cognitive phenotype measures for psychomotor speed, general cognitive ability, cognitive control, response inhibition, task switching, spatial attention, nonverbal reasoning, and fluid intelligence.

In addition, we identified a wide range of physiological, physical, and behavioral phenotypes distinct for either the cortex or the cerebellum latent variables. Walking and other vigorous physical activities yielded more significant *P* values for the cerebellum, but time spent watching TV and length of phone usage, which are both sedentary behaviors that add to the risks of weight gain and obesity, were more related to the cortex. Interestingly, the phenotypes uniquely linked to the cerebellum, as opposed to the cortex, are largely general physical properties such as height, fat-free mass (FFM), and hand grip strength. Instead, measurements of body fat (or fat mass) are unique to the cortex. Diastolic blood pressure (DBP) and ventricular rate (heart rate) were uniquely associated with the cerebellum but systolic blood pressure (SBP) and carotid intima-media thickness (CIMT) that is a measure used to diagnose the extent of carotid atherosclerotic vascular disease were related to the cortex. Finally, alcohol intake was solely associated with the cortex.

In fact, the blood traits also displayed a coherent link with variation in the cortex and for the cerebellum separately. For the cerebellum, several red blood cell-related phenotypes are highly significant (e.g., hemoglobin concentration, mean corpuscular volume/hemoglobin/concentration, and hematocrit percentage). Other associated phenotypes included urate (or uric acid) related to kidney function, monocyte and leukocyte (both are white blood cell) count, γ-glutamyl transferase (GGT, related to the liver), and reticulocyte (immature red blood cells) count and percentage. On the contrary, the phenotypes observed only for the cortex included glycated hemoglobin (HbA1c, diabetes), basophil (a white blood cell mainly participating in allergic and inflammatory reactions) count, low-density lipoprotein (LDL-cholesterol or "bad" cholesterol), and Apolipoprotein B (ApoB, cardiovascular disease). This observation also seemed to go hand in hand with more physical activity associated with the cerebellum, therefore increased angiogenesis and blood cells (85), but more sedentary behaviors in the cortex, which is associated with increased risk of diabetes (86, 87), obesity, and

cardiovascular diseases. Interestingly, insulin growth factor 1 (IGF-1) showed equal association with the cortex and the cerebellum.

Funct7net *Mode 2*'s Phenotype Array is Driven by Time Spent Watching TV

In *mode 2* (Funct7net, Fig. 5), which separates the visual attention system from other higher-order neural systems, the driving phenotype for the cortex is time spent watching TV that surpassed other phenotypes by magnitudes. It is also among the top phenotypes associated with the cerebellum. Sleep-related phenotypes such as sleep duration and nap during the day were more related to the cortex than the cerebellum while snoring was more related to the cerebellum. Alcohol was mostly related to the cortex but also has a significant link with variation in the cerebellum pattern.

The cognitive phenotypes that were significant were again fluid intelligence with a focus on linguistic and arithmetic ability (FI1: numeric addition test, FI4: positional arithmetic, FI3: word interpolation, FI7: synonym, and FI6: conditional arithmetic) and initial answer for prospective memory. Their associations with the cortex and the cerebellum were more equivalent than in *mode 1*.

Furthermore, the body mass index (BMI), height, blood assay, and cardiac phenotypes were more uniquely related to the cortex, possibly because the *mode 2*'s cerebellar latent variables only emphasized some regions (Funct7net, Fig. 1*B*) instead of the entire cerebellum. It is also possible that even if some phenotypes showed more association with the cortex or the cerebellum across modes, these phenotypes were related to both the cortex and cerebellum. For example, the hemoglobin concentration and hematocrit percentage could be linked to both the areas in the cortex and the cerebellum. Thus, we do not discuss them again.

Most Brain-Trait Links Are Congruent between Funct7net and Funct100region *Modes 1* and *2*

Given the similarity of modes between Funct7net and Funct100region, especially for the cerebellar variation, we expected to see a similar phenotype signature in Funct100region *modes 1*, *2* (Supplemental Figs. S5 and S6) compared with Funct7net *modes 1* and *2* (Figs. 4 and 5). Indeed, most phenotypes were congruent.

However, for the cortical latent variable of Funct100region *mode 1*, we observed several differences. First, the cortical association with IGF-1 was the strongest. HbA1c, basophil count, and LDL were uniquely associated with the cortex, but the associations were much smaller. IGF-1 has an important role in brain development, neuroplasticity, and neuroprotection after brain injury. Expiratory measurement (peak expiratory flow [PEF] and forced expiratory volume in 1 s [FEV1]) were more related to the cortex than the cerebellum, possibly because of oxygenation in brain structure and function. Systolic blood pressure and carotid intima-media thickness measures were insignificant.

Finally, time spent watching TV was associated more with the cerebellum than the cortex, along with physical activity (walking, climbing stairs), which was not observed in Funct7net *mode 1*. Phone usage was also not significant. Because the cortical latent variable in Funct100region *mode 1* emphasized mostly the associative regions between the sensorimotor system and higher-cognitive system, the cognitive phenotypes were uninterrupted.

Funct100region *Mode 3* Phenotype Profiles' Link to Ipsilateral Brain Patterns Were Hidden

In Funct100region *mode 3*, where we see the ipsilateral cerebellar-cortical correspondence, most significant phenotypes showed stronger associations with the cortex than with the cerebellum. These significant phenotypes include TMT-A/B, number of siblings, ventricular/pulse rate, reticulocytes counts/percentages, tobacco smoking, IGF-1, handedness, FI3: word interpolation, corpuscular hemoglobin as well as matrix completion—an aspect of IQ testing (Supplemental Fig. S9).

DISCUSSION

Overview

The cerebellar and cerebral cortex closely interact in supporting everyday activities, from body movement to solving complex problem solving (8, 14, 88, 89). Yet, it remains mysterious how different parts of these two structures work hand in hand with each other (72, 90). Here, we designed a mission-tailored analytical framework to 38,527 UKBB participants' regional gray matter volumes to analyze multiple cerebellum-cortex population covariation patterns and understand how these patterns relate to 977 phenotypic measurements. The most explanatory population mode exhibited the anticorrelation between higher-order cognitive networks (except dorsal attention network) and low-level visual-sensorimotor network within the cerebellum, which mirrors the cortex. The second mode revealed a contrast between the visual attention system and other higher-order cognitive system, especially the DMN and limbic system. Another mode revealed an interesting but puzzling ipsilateral structural covariation pattern, despite the mainly contralateral ties between the cerebral and cerebellar cortex. Finally, the phenotypic profiles of the most explanatory patterns unveiled an array of real-world implications with mind, body, and exposure of everyday life.

One important finding of this paper was that the functional parcellation explains the structural covariation across individuals better than structural parcellation, especially in the most explanatory modes. This is somewhat surprising, as regions in the functional parcellation often are spatially discontinuous, consisting of multiple parts. If anatomical variation was simply spatially correlated, the more contiguous anatomical parcellation should have performed better. The results imply that not only functional boundaries (64), but also anatomical variation, are better described using functionally defined regions, and that there is value in not respecting lobular microanatomical boundaries.

The uniform cytoarchitecture across the whole cerebellar cortex is well-established (25, 91–93). Despite what appears like an anatomical fact, it has been suspected before that circumscribed territories in the cerebellum have privileged relationships to specific parts of the brain (2, 13, 14, 73, 94, 95). Even more so, the cerebellum may harbor a homotopic map of the cerebral cortex (9). Our findings confirm and

extend this contention. In addition, we recontextualize the increasing recognition of a cortical high-low gradient of neural systems given that specific parts of the cerebellum are reliably mapped to both low-level sensorimotor and high-level cognitive cortical systems.

Visual Attentional Representation in the Cerebellum Mirrors That in the Cerebral Cortex

The strong contribution of the visual system in *mode 1* and *2* is particularly interesting (Figs. 1 and 2 and Supplemental Fig S1, *A* and *B* and Fig. S2, *A* and *B*). Although the primary visual representation remained traditionally undetected and was conceptually denied in earlier brain-imaging research on the human cerebellum based on resting-state functional connectivity (9), recently, van Es et al. (96) identified three distinct visual spatial representations in the cerebellum (oculomotor vermis, lobule VIIb, and lobule VIIIb). In resting-state fMRI data from human connectome project (HCP), Guell et al. (97) identified a representation of the "visual functional territory" that was separated from other functional territories of the human dentate nucleus. Xue et al. (98) recently confirmed the early retinotopic visual cortex representation in detailed cerebellar parcellation in three human subjects. Our present results add evidence that speak to a visual cortical representation in the cerebellum, from the novel angle of structural covariation at the population level.

Furthermore, King et al. (64) also treated lobule VI vermis as a region related to complex saccades that require attentional control. Indeed, there is some evidence that the DAN and the visual network representation can be closely associated in the cerebellum (11, 70). King et al. (11) showed that the oculomotor vermis of the cerebellum is predicted best by neural activity responses of regions in DAN and extrastriate visual cortex. Brissenden et al. (99) also showed visual field representation in lobule VIIb/VIIIa that mirrors a portion of IPS, which is considered part of the DAN. Moreover, the DAN has a close relationship with sensorimotor regions and serves a key role in the visuospatial perceptual attention (100–103).

We note that the DAN was virtually absent from *mode 1* (Funct7net, Struct7net, and Funct100region). DAN also had opposite ties to other higher-order cognitive networks in *mode 2* (Funct7net, Struct7net, and Funct100region). These higher-order cognitive systems included the default mode network (DMN), ventral salience network (VSN), limbic network, and executive control network (ECN). Although there is abundant evidence that DAN exhibited a different pattern compared with other higher-order cognitive systems in the cerebral cortex, our present findings suggest that DAN might also be anchored in a unique way in the cerebellum compared with the other higher-order cognitive systems. Cortical DAN and default mode network (DMN) typically show anticorrelated relationships, which has been widely recognized as a general feature of human brain organization (68, 69, 71). Our findings suggest that this antagonistic relationship may also manifest in the human cerebellum.

Ipsilateral Cerebellum-Cortex Correspondence in Humans Can Be Important

Whereas cerebellum-cortex communications are usually portrayed as contralateral, our findings in *mode 3* (Funct100region) identified underappreciated ipsilateral cerebrocerebellar interactions. The feedforward pathways linking cerebral cortex to cerebellum are conveyed in cortico-pontocerebellar (CPC) projections that originate from the frontal, temporal, parietal, and occipital lobes of the cerebral cortex, and terminate on nuclei of the ipsilateral basis pontis. Pontocerebellar axons then traverse the pons to enter the contralateral middle cerebellar peduncle and course to the contralateral cerebellum. Notably, up to 30% of these axons cross again in the cerebellar white matter to terminate on the cerebellum on the same side as the cerebral cortical areas of origin (104, 105). The feedback pathways from cerebellum to cerebral cortex are conveyed in the dentato-rubro-thalamo-cortical tracts (DRTT or DRTC) that originate in the deep cerebellar nuclei (dentate nucleus, but also the fastigial and the interposed—globose and emboliform nuclei), course in the superior cerebellar peduncle, decussate in the brachium conjunctivum, pass through the contralateral red nucleus to which they provide passing collaterals, and then ascend to terminate in a discrete set of nuclei in the thalamus. The thalamocortical projections close the feedback circuit (106). We demonstrate the cerebrocerebellar tracts in Fig. 6. Anatomical tract tracing studies in animals show that the major connections between the cerebellum and cerebral cortex are contralateral (5, 8, 107–109), although there are some ipsilateral or nondecussating DRTT (nd-DRTT) pathways in monkeys (109, 110), cats (111), and ∼20% ipsilateral DRTT and pontocerebellar pathways in rats (112–114). As argued by Doron et al. (115) and others, assumptions about anatomical connections in the human brain inferred from the tract-tracing studies performed in monkeys should be considered with care, as the association cortices are more developed and may project more to the cerebellum in humans than in animals (116, 117).

Ipsilateral pathways are evident also in studies of the human cerebellum. In the feedforward system, diffusion tensor imaging (DTI) studies suggest that there are ipsilateral CPC tracts, traveling from the temporal lobe, occipital lobe (118–121), and parietal lobe (119, 120) to the cerebellum. Microsurgical human postmortem brain microdissections of the feedback projection reveal an nd-DRTT pathway (122, 123), and DTI fiber tract reconstructions in the living brain identified an nd-DRTT pathway accounting for one-fifth of the overall DRTT (119, 120, 122, 124). Our own data would be in line with these ipsilateral cerebellum-cortex correspondences (Fig. 3). Despite DTI's ability to reconstruct the major contralateral feedforward and feedback pathways (118–120, 122, 124, 125), it is inherently limited in resolving crossing and kissing fibers. Thus, the interpretation of DTI results can be challenging (126) and this may impact statements on hemispheric asymmetry. Support for the ipsilateral connectivity in humans, however, comes from brain stimulation studies. Repetitive transcranial magnetic stimulation (rTMS) and transcranial direct current stimulation (tDCS) on one side of the cerebellum produce strong bilateral effects on fMRI or PET studies of motor tasks (127) and verbal working memory retrieval tasks (128) as well as brain-wide cortical metabolism (129). Admittedly, bilateral cortical activation in the case of unilateral cerebellar stimulation could also result from interhemispheric communication happening at the

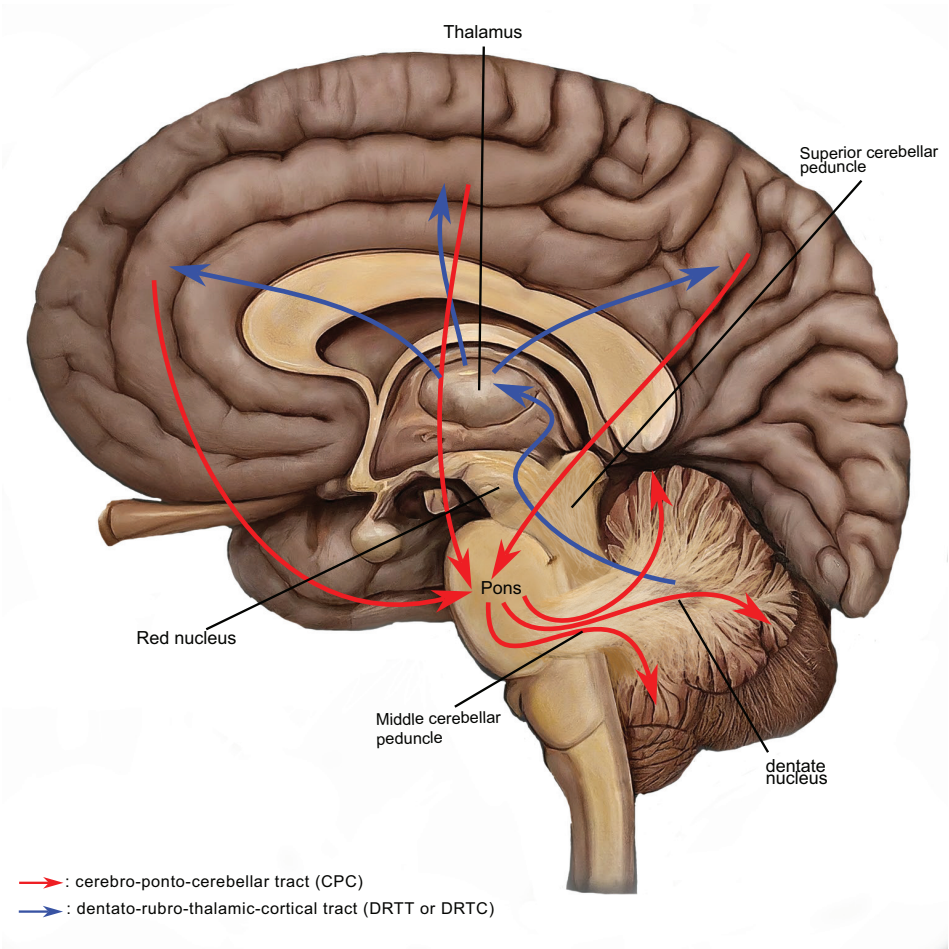

Figure 6. The feedforward and feedback pathways between the cerebellum and the cerebral cortex based on an example of the right side of the brain, where the right is considered ipsilateral while the left is considered contralateral. The feedforward pathway or cortico-ponto-cerebellar (CPC) tracts begins in the right cerebral cortex, projecting to the ipsilateral (same side) pontine nuclei. Axons then cross the midline to the contralateral (opposite side) middle cerebellar peduncle, reaching the contralateral cerebellum shown here in the sagittal cross section. Some axons cross the midline again within the cerebellum to innervate the ipsilateral cerebellum. Conversely, the feedback pathway or dentato-rubro-thalamo-cortical tracts (DRTT or DRTC) originate in the deep cerebellar nuclei, specifically the left dentate nucleus in this example. It travels through the contralateral superior cerebellar peduncle, mainly decussating to the ipsilateral red nucleus, before ascending to terminate in the ipsilateral thalamus. In addition, nondecussating collaterals pass through the contralateral red nucleus to terminate in the contralateral thalamus. The thalamocortical projections close the feedback circuit.

cortical level, driven by changes in the contralateral cerebral hemisphere that was directly influenced by the stimulated side of the cerebellum. Alternatively, it has been suggested that this bilateral activation could also be compensatory for reduced contralateral cortical activation because of purported cerebellar inhibition, depending on the type of tDCS applied (130). Furthermore, in resting-state functional connectivity studies in humans, Igelstrom et al. (131) noted functional connectivity between seed regions on one side of the temporoparietal junction (TPJ) and bilateral areas in lobules V, VI, crus I/II, lobule VIIIa/b, and IX. The emphasis was on the contralateral side, but the ipsilateral functional connectivity between each seed region and cerebellum was prominent. In complement to cerebral cortical seeds, relevant previous research (132, 133) reported multiple unilateral cerebellar seed regions (right lobule I–IV, V, VI, crus I, VIIIa, IX, X, dorsal and ventral dentate nucleus) showing functional connectivity with corresponding bilateral cerebral cortical regions, further supporting the notion of ipsilateral connectivity.

Our ipsilaterally patterned modes document ipsilateral correspondence underlying the population covariation between the cerebellum and the cortex on a large scale. Our structural covariation approach is applicable at the whole brain level and unchangeable because it is applied purely to structural data and independent of the experiments or subject outliers. This provides a degree of confidence in the validity of the observations, the significance of which remains to be determined in future research.

PheWAS Revealed Distinct Cerebellar and Cortical Phenotypic Profiles for Each Mode

Our PheWAS has screened a diverse palette of phenotypic indicators to delineate their associations with our derived cortical and cerebellar brain patterns. Within each mode, numerous phenotypes associated with either cortical or cerebellar latent variables have also demonstrated significant brain-behavior links.

For the cerebellar *mode 1* (Funct7net and Funct100region; Fig. 6), we found the cognitive phenotypes measuring psychomotor speed, physical activity, fat-free mass, hand grip strength, blood cell metrics, and cardiovascular measurement to be particularly relevant. The cognitive tests indexing psychomotor processing speed (e.g., reaction time, DSST, and TMT-A) and hand grip strength showed robust and significant association with the cerebellar *mode 1*. The strong association between these phenotypes was reported in another UKBB study (134). Multiple studies across different populations indicated physical exercise is positively correlated with cerebellar gray matter volume (135, 136), gray matter mean diffusivity (137), and network connectivity (138) coupled with improved cognitive performance. In rats, exercise induces angiogenesis in the cerebellum, which resonates with our strong association between blood cells (red

blood cells, white blood cells, reticulocytes, and IGF-1) and cerebellum (85, 139, 140). However, γ-glutamyl transferase (GGT) and urate's association in our findings with the cerebellum was unclear. The cerebellum is thought to assist in regulating autonomic functions such as heart rate, respiration, and sleep-wake cycle through hindbrain projections from parabrachial nuclei (PBN) (72, 141–149). Thus, diastolic blood pressure (DBP) and ventricular rate could indeed be associated with individual differences in cerebellar morphology. In cerebellar *mode 2* (Funct7net), we also identified sleep-related phenotypes and snoring, which could be regulated through this pathway as well (141, 150–152). Previous studies observed a relationship between height and cerebellum volume in adults (153–156). Similarly, BMI has strong associations with gray matter volume in middle-aged and older adults, including the cerebellum (157–160). In particular, Weise et al. (161) found that although both fat mass and fat-free mass (FFM) contribute to BMI, they have differential impacts on brain structure, including a negative association between cerebellar GMV and fat mass, but not FFM. Since FFM consists mainly of skeletal muscle, bones, and parenchymal organs that are metabolically active, this echoes a close link of exercise with the cerebellum, in line with our analysis.

For the cortical *mode 1* (Funct7net), the various cognitive phenotypes related to abstract reasoning, executive functions, focused visual attention, and motor control confirm the known functions of the cerebral cortex, and highlight other phenotypes including time spent watching TV, fat mass, blood indicators of diabetes, immunoreactions, and cardiovascular disease. For example, TV consumption played an important role in both *mode 1* and *mode 2* (Funct7net). TV consumption is both a sedentary and passive-receptive behavior. For *mode 1*, a wide range of studies have shown that excessive TV watching was negatively correlated with gray matter volume in multiple cortical regions and cognitive functions in both the young and elderly (162–164) but positively correlated with risks of type 2 diabetes, cardiovascular diseases, and increased BMI (165, 166), despite physical activity (167, 168). The blood traits are strongly confirmatory of these results, as we saw HbA1c that measures blood sugar level and is a marker for diabetes. We here also observed LDL and ApoB links, which were highly associated with sedentary time (169) and are important predictors of cardiovascular diseases (170–172). In addition, elevated basophil count was reported in some patients with diabetes (173) and patients with coronary artery disease (174). The effects of basophil might be related to adiposity-associated inflammatory factors (175). Finally, systolic blood pressure and carotid intima-media thickness show significant association with the cerebral cortex, which is consistently observed across different types of studies and populations (176–179). Interestingly, high lipoprotein levels and diabetes as seen in blood traits for the cortex, obesity, and a sedentary lifestyle as seen in physical and lifestyle phenotypes for the cortex, all contribute to the thickening of carotid intima-media.

For the cortical *mode 2* (Funct7net; Supplemental Fig. S5), which separates the visual attention system from other higher-order cognitive systems (cf. aforementioned), we identified watching TV as the leading phenotype associated with both the cortex and the cerebellum—potentially another piece of evidence for complex behaviors being related to the cerebellum. Apart from being sedentary, watching TV's more receptive nature differentiates it from behaviors such as reading or gaming. Many observed that watching TV activated key nodes in DMN and suppressed DAN (180, 181) that is coherent with our interpretation of *mode 2* (Funct7net) that this mode reflects the anticorrelation between DAN and DMN. In fact, attentional deficits were often observed in children and adolescents with too much TV exposure (182–184). At the same time, one receives abundant visual and narrative stimuli while watching TV, which is directly associated with the visual system and with semantic processing in association cortex (185). Thus, cerebellar structural brain variation can be expected to be jointly reflected in visual and association cortices, an idea that receives support from a cross-sectional study on TV viewing and brain structure (162).

In contrast to *mode 1*, *mode 2*'s significant cognitive phenotypes mostly relate to fluid intelligence tests and prospective memory. Both faculties closely implicate executive functions and working memory, which are supported by the visual-attention system (186–189). Moreover, the fluid intelligence tests were characterized by arithmetical tasks, which demand effortful top-down visual attentional control (190).

In both *modes 1* and *2* (Funct7net), we noticed smartphone usage was most associated with cerebral cortex variation. Excessive smartphone usage is related to altered structures in frontal, temporal, insular, and anterior cingulate regions and reduced neural activity responses when viewing emotional stimulus in fronto-cingulate regions (191–194). These regions were implicated in cerebellar-cortical population modes as part of the higher cognitive systems that stands in some antagonistic contrast with lower sensorimotor system.

Conclusions

Our first two modes are consistent with the DMN-visuomotor divergence of neural systems, as well as the classical double motor representation and the recently proposed triple nonmotor representation in the cerebellum. Our results support the anticorrelation between visual-attention and other higher-order cognitive systems in the cerebellum, like in the cortex. Our third mode indicates a greater proportion of ipsilateral mechanisms between the cerebellum and cortex that may be overshadowed by the more abundant contralateral pathways. The distinct phenotype profiles for each mode and their latent variables revealed unique brain phenomena—behavior links that weighed differently in the cerebellum and the cortex. These findings greatly contribute to our understanding of the intricate interplay among the cortex, cerebellum, and behaviors.

Limitations

Currently, the analysis was done on a cross-sectional cohort and left out the subcortical systems. There has been an increasing interest and understanding in the cortico-subcortico-cerebellar interactions underpinning multiple critical functions and diseases across lifespan (195–201). In the current analysis, we did not include the subcortical systems mainly due to worse brain imaging signal quality compared

with the cerebral cortex and the cerebellum, which may have skewed our analyses. In the future, we plan to investigate the longitudinal effect of cerebellar-cortical structural covariation and potentially study the subcortico-cerebellar interactions to obtain a more complete picture.

DATA AVAILABILITY

All data from UK Biobank are available to other investigators online (ukbiobank.ac.uk). The Schaefer-Yeo cerebral cortical atlas is accessible online (https://github.com/ThomasYeoLab/CBIG/tree/master/stable_projects/brain_parcellation/Schaefer2018_LocalGlobal). The functional cerebellum atlas is accessible online (https://github.com/DiedrichsenLab/cerebellar_atlases/tree/master/Nettekoven_2023).

SUPPLEMENTAL MATERIAL

Supplemental Figs. S1–S9: https://doi.org/10.17605/OSF.IO/V7KF9.

Supplemental Tables S1–S3: https://doi.org/10.17605/OSF.IO/V7KF9.

GRANTS

B.T.T.Y. is supported by the NUS Yong Loo Lin School of Medicine Grant NUHSRO/2020/124/TMR/LOA, the Singapore National Medical Research Council (NMRC) LCG Grant OFLCG19May-0035, NMRC CTG-IIT Grant CTGIIT23jan-0001, NMRC STaR Grant STaR20nov-0003, Singapore Ministry of Health (MOH) Centre Grant CG21APR1009, the Temasek Foundation Grant TF2223-IMH-01, and the United States National Institutes of Health Grants R01MH120080 and R01MH133334.

DISCLAIMERS

Any opinions, findings and conclusions or recommendations expressed in this material are those of the authors and do not reflect the views of the Singapore NMRC, MOH, or Temasek Foundation.

DISCLOSURES

No conflicts of interest, financial or otherwise, are declared by the authors.

AUTHOR CONTRIBUTIONS

Z.W., J.D., K.S., C.S., S.R.A.A., and D.B. conceived and designed research; Z.W. performed experiments; Z.W., J.D., K.S., C.S., S.R.A.A., B.T.T.Y., J.D.S. and D.B. analyzed data; Z.W., J.D., K.S., C.S., S.R.A.A., B.T.T.Y., J.D.S., and D.B. interpreted results of experiments; Z.W., J.D., K.S., and D.B. prepared figures; Z.W. and D.B. drafted manuscript; Z.W., J.D., K.S., C.S., S.R.A.A., B.T.T.Y., J.D.S., and D.B. edited and revised manuscript; Z.W., J.D., K.S., C.S., S.R.A.A., B.T.T.Y., J.D.S., and D.B. approved final version of manuscript.

REFERENCES

1. **Leiner HC**, **Leiner AL**, **Dow RS.** Reappraising the cerebellum: what does the hindbrain contribute to the forebrain? *Behav Neurosci* 103: 998–1008, 1989. doi:10.1037//0735-7044.103.5.998.
2. **Schmahmann JD.** An emerging concept: the cerebellar contribution to higher function. *Arch Neurol* 48: 1178–1187, 1991. doi:10.1001/archneur.1991.00530230086029.
3. **Schmahmann JD**, **Pandya DN.** Anatomical investigation of projections to the basis pontis from posterior parietal association cortices in rhesus monkey. *J Comp Neurol* 289: 53–73, 1989. doi:10.1002/cne.902890105.
4. **Schmahmann JD**, **Pandya DN.** Projections to the basis pontis from the superior temporal sulcus and superior temporal region in the rhesus monkey. *J Comp Neurol* 308: 224–248, 1991. doi:10.1002/cne.903080209.
5. **Schmahmann JD**, **Pandya DN.** Anatomic organization of the basilar pontine projections from prefrontal cortices in rhesus monkey. *J Neurosci* 17: 438–458, 1997. doi:10.1523/JNEUROSCI.17-01-00438.1997.
6. **Middleton FA**, **Strick PL.** Cerebellar projections to the prefrontal cortex of the primate. *J Neurosci* 21: 700–712, 2001. doi:10.1523/JNEUROSCI.21-02-00700.2001.
7. **Middleton FA**, **Strick PL.** Anatomical evidence for cerebellar and basal ganglia involvement in higher cognitive function. *Science* 266: 458–461, 1994. doi:10.1126/science.7939688.
8. **Kelly RM**, **Strick PL.** Cerebellar loops with motor cortex and prefrontal cortex of a nonhuman primate. *J Neurosci* 23: 8432–8444, 2003. doi:10.1523/JNEUROSCI.23-23-08432.2003.
9. **Buckner RL**, **Krienen FM**, **Castellanos A**, **Diaz JC**, **Yeo BT.** The organization of the human cerebellum estimated by intrinsic functional connectivity. *J Neurophysiol* 106: 2322–2345, 2011. doi:10.1152/jn.00339.2011.
10. **Ji JL**, **Spronk M**, **Kulkarni K**, **Repovš G**, **Anticevic A**, **Cole MW.** Mapping the human brain's cortical-subcortical functional network organization. *NeuroImage* 185: 35–57, 2019. doi:10.1016/j.neuroimage.2018.10.006.
11. **King M**, **Shahshahani L**, **Ivry RB**, **Diedrichsen J.** A task-general connectivity model reveals variation in convergence of cortical inputs to functional regions of the cerebellum. *eLife* 12: e81511, 2023. doi:10.7554/eLife.81511.
12. **Guell X**, **Gabrieli JDE**, **Schmahmann JD.** Triple representation of language, working memory, social and emotion processing in the cerebellum: convergent evidence from task and seed-based resting-state fMRI analyses in a single large cohort. *NeuroImage* 172: 437–449, 2018. doi:10.1016/j.neuroimage.2018.01.082.
13. **Schmahmann JD.** From movement to thought: anatomic substrates of the cerebellar contribution to cognitive processing. *Hum Brain Mapp* 4: 174–198, 1996. doi:10.1002/(SICI)1097-0193(1996)4:3<174::AID-HBM3>3.0.CO;2-0.
14. **Schmahmann JD**, **Guell X**, **Stoodley CJ**, **Halko MA.** The theory and neuroscience of cerebellar cognition. *Annu Rev Neurosci* 42: 337–364, 2019. doi:10.1146/annurev-neuro-070918-050258.
15. **Saleeba C**, **Dempsey B**, **Le S**, **Goodchild A**, **McMullan S.** A student's guide to neural circuit tracing. *Front Neurosci* 13: 897, 2019 [Erratum in Front Neurosci 14: 177, 2020]. doi:10.3389/fnins.2019.00897.
16. **Li J**, **Liu T**, **Dong Y**, **Kondoh K**, **Lu Z.** Trans-synaptic neural circuit-tracing with neurotropic viruses. *Neurosci Bull* 35: 909–920, 2019. doi:10.1007/s12264-019-00374-9.
17. **Osten P**, **Margrie TW.** Mapping brain circuitry with a light microscope. *Nat Methods* 10: 515–523, 2013. doi:10.1038/nmeth.2477.
18. **Bohland JW**, **Wu C**, **Barbas H**, **Bokil H**, **Bota M**, **Breiter HC et al**. A proposal for a coordinated effort for the determination of brainwide neuroanatomical connectivity in model organisms at a mesoscopic scale. *PLoS Comput Biol* 5: e1000334, 2009. doi:10.1371/journal.pcbi.1000334.
19. **Preuss TM**, **Cáceres M**, **Oldham MC**, **Geschwind DH.** Human brain evolution: insights from microarrays. *Nat Rev Genet* 5: 850–860, 2004. doi:10.1038/nrg1469.
20. **Van Essen DC**, **Dierker DL.** Surface-based and probabilistic atlases of primate cerebral cortex. *Neuron* 56: 209–225, 2007. doi:10.1016/j.neuron.2007.10.015.
21. **Sherwood CC**, **Bauernfeind AL**, **Bianchi S**, **Raghanti MA**, **Hof PR.** Human brain evolution writ large and small. *Prog Brain Res* 195: 237–254, 2012. doi:10.1016/B978-0-444-53860-4.00011-8.
22. **Hill J**, **Inder T**, **Neil J**, **Dierker D**, **Harwell J**, **Van Essen D.** Similar patterns of cortical expansion during human development and evolution. *Proc Natl Acad Sci USA* 107: 13135–13140, 2010. doi:10.1073/pnas.1001229107.
23. **Balsters JH**, **Cussans E**, **Diedrichsen J**, **Phillips KA**, **Preuss TM**, **Rilling JK**, **Ramnani N.** Evolution of the cerebellar cortex: the selective expansion of prefrontal-projecting cerebellar lobules. *NeuroImage* 49: 2045–2052, 2010. doi:10.1016/j.neuroimage.2009.10.045.

24. **Leiner HC**, **Leiner AL**, **Dow RS.** Does the cerebellum contribute to mental skills? *Behav Neurosci* 100: 443–454, 1986. doi:10.1037//0735-7044.100.4.443.
25. **Buckner RL.** The cerebellum and cognitive function: 25 years of insight from anatomy and neuroimaging. *Neuron* 80: 807–815, 2013. doi:10.1016/j.neuron.2013.10.044.
26. **Leiner HC**, **Leiner AL**, **Dow RS.** Cognitive and language functions of the human cerebellum. *Trends Neurosci* 16: 444–447, 1993. doi:10.1016/0166-2236(93)90072-t.
27. **Whiting BA**, **Barton RA.** The evolution of the cortico-cerebellar complex in primates: anatomical connections predict patterns of correlated evolution. *J Hum Evol* 44: 3–10, 2003. doi:10.1016/s0047-2484(02)00162-8.
28. **Liu X**, **d'Oleire Uquillas F**, **Viaene AN**, **Zhen Z**, **Gomez J.** A multifaceted gradient in human cerebellum of structural and functional development. *Nat Neurosci* 25: 1129–1133, 2022. doi:10.1038/s41593-022-01136-z.
29. **Gaiser C**, **van der Vliet R**, **de Boer AAA**, **Donchin O**, **Berthet P**, **Devenyi GA**, **Chakravarty MM**, **Diedrichsen J**, **Marquand AF**, **Frens MA**, **Muetzel RL.** Large data on the small brain: population-wide cerebellar growth models of children and adolescents (Preprint). *bioRxiv*, 2023. doi:10.1101/2023.04.26.538263.
30. **Kipping JA**, **Tuan TA**, **Fortier MV**, **Qiu A.** Asynchronous development of cerebellar, cerebello-cortical, and cortico-cortical functional networks in infancy, childhood, and adulthood. *Cereb Cortex* 27: 5170–5184, 2016. doi:10.1093/cercor/bhw298.
31. **Schmahmann JD**, **Doyon J**, **Toga AW**, **Petrides M**, **Evans AC.** *MRI Atlas of the Human Cerebellum*. San Diego, CA: Academic Press, 2000.
32. **Angevine JB**, **Mancall EL**, **Yakovlev PI.** The human cerebellum, an atlas of gross topography in serial sections. *Neurology* 13: 179–179-b, 1963. doi:10.1212/WNL.13.2.179-b.
33. **Schlerf JE**, **Verstynen TD**, **Ivry RB**, **Spencer RMC.** Evidence of a novel somatopic map in the human neocerebellum during complex actions. *J Neurophysiol* 103: 3330–3336, 2010. doi:10.1152/jn.01117.2009.
34. **Snider RS**, **Stowell A.** Receiving areas of the tactile, auditory, and visual systems in the cerebellum. *J Neurophysiol* 7: 331–357, 1944. doi:10.1152/jn.1944.7.6.331.
35. **Grodd W**, **Hülsmann E**, **Lotze M**, **Wildgruber D**, **Erb M.** Sensorimotor mapping of the human cerebellum: fMRI evidence of somatotopic organization. *Hum Brain Mapp* 13: 55–73, 2001. doi:10.1002/hbm.1025.
36. **Habas C**, **Axelrad H**, **Cabanis E-A.** The cerebellar second homunculus remains silent during passive bimanual movements. *Neuroreport* 15: 1571–1574, 2004. doi:10.1097/01.wnr.0000133970.53139.e3.
37. **Habas C**, **Axelrad H**, **Nguyen T**, **Cabanis E-A.** Specific neocerebellar activation during out-of-phase bimanual movements. *Neuroreport* 15: 595–599, 2004. doi:10.1097/00001756-200403220-00005.
38. **Nitschke MF**, **Kleinschmidt A**, **Wessel K**, **Frahm J.** Somatotopic motor representation in the human anterior cerebellum. *Brain* 119: 1023–1029, 1996. doi:10.1093/brain/119.3.1023.
39. **Rijntjes M**, **Buechel C**, **Kiebel S**, **Weiller C.** Multiple somatotopic representations in the human cerebellum. *Neuroreport* 10: 3653–3658, 1999. doi:10.1097/00001756-199911260-00035.
40. **Thickbroom GW**, **Byrnes ML**, **Mastaglia FL.** Dual representation of the hand in the cerebellum: activation with voluntary and passive finger movement. *NeuroImage* 18: 670–674, 2003. doi:10.1016/s1053-8119(02)00055-1.
41. **Alfaro-Almagro F**, **Jenkinson M**, **Bangerter NK**, **Andersson JLR**, **Griffanti L**, **Douaud G**, **Sotiropoulos SN**, **Jbabdi S**, **Hernandez-Fernandez M**, **Vallee E**, **Vidaurre D**, **Webster M**, **McCarthy P**, **Rorden C**, **Daducci A**, **Alexander DC**, **Zhang H**, **Dragonu I**, **Matthews PM**, **Miller KL**, **Smith SM.** Image processing and Quality Control for the first 10,000 brain imaging datasets from UK Biobank. *NeuroImage* 166: 400–424, 2018. doi:10.1016/j.neuroimage.2017.10.034.
42. **Miller KL**, **Alfaro-Almagro F**, **Bangerter NK**, **Thomas DL**, **Yacoub E**, **Xu J**, **Bartsch AJ**, **Jbabdi S**, **Sotiropoulos SN**, **Andersson JL**, **Griffanti L**, **Douaud G**, **Okell TW**, **Weale P**, **Dragonu I**, **Garratt S**, **Hudson S**, **Collins R**, **Jenkinson M**, **Matthews PM**, **Smith SM.** Multimodal population brain imaging in the UK Biobank prospective epidemiological study. *Nat Neurosci* 19: 1523–1536, 2016. doi:10.1038/nn.4393.
43. **Smith SM.** Fast robust automated brain extraction. *Hum Brain Mapp* 17: 143–155, 2002. doi:10.1002/hbm.10062.
44. **Jenkinson M**, **Bannister P**, **Brady M**, **Smith S.** Improved optimization for the robust and accurate linear registration and motion correction of brain images. *NeuroImage* 17: 825–841, 2002. doi:10.1016/s1053-8119(02)91132-8.
45. **Jenkinson M**, **Smith S.** A global optimisation method for robust affine registration of brain images. *Med Image Anal* 5: 143–156, 2001. doi:10.1016/s1361-8415(01)00036-6.
46. **Andersson JL**, **Jenkinson M**, **Smith S.** *Non-Linear Registration, aka Spatial Normalisation*. FMRIB technical report TR07JA2. Oxford, UK: FMRIB Analysis Group of the University of Oxford, 2007, vol. 2, p. e21.
47. **Zhang Y**, **Brady M**, **Smith S.** Segmentation of brain MR images through a hidden Markov random field model and the expectation-maximization algorithm. *IEEE Trans Med Imaging* 20: 45–57, 2001. doi:10.1109/42.906424.
48. **Smith SM**, **Zhang Y**, **Jenkinson M**, **Chen J**, **Matthews PM**, **Federico A**, **De Stefano N.** Accurate, robust, and automated longitudinal and cross-sectional brain change analysis. *NeuroImage* 17: 479–489, 2002. doi:10.1006/nimg.2002.1040.
49. **Schaefer A**, **Kong RU**, **Gordon EM**, **Laumann TO**, **Zuo X-N**, **Holmes AJ**, **Eickhoff SB**, **Yeo BTT.** Local-global parcellation of the human cerebral cortex from intrinsic functional connectivity MRI. *Cereb Cortex* 28: 3095–3114, 2018. doi:10.1093/cercor/bhx179.
50. **Diedrichsen J**, **Balsters JH**, **Flavell J**, **Cussans E**, **Ramnani N.** A probabilistic MR atlas of the human cerebellum. *NeuroImage* 46: 39–46, 2009. doi:10.1016/j.neuroimage.2009.01.045.
51. **Zhi D**, **Shahshahani L**, **Nettekoven C**, **Pinho AL**, **Bzdok D**, **Diedrichsen J.** A hierarchical Bayesian brain parcellation framework for fusion of functional imaging datasets (Preprint). *bioRxiv*, 2023. doi:10.1101/2023.05.24.542121.
52. **Nettekoven C**, **Zhi D**, **Shahshahani L**, **Pinho AL**, **Saadon-Grosman N**, **Diedrichsen J.** A hierarchical atlas of the human cerebellum for functional precision mapping (Preprint). *bioRxiv*, 2023. doi:10.1101/2023.09.14.557689.
53. **Spreng RN**, **Dimas E**, **Mwilambwe-Tshilobo L**, **Dagher A**, **Koellinger P**, **Nave G**, **Ong A**, **Kernbach JM**, **Wiecki TV**, **Ge T**, **Li Y**, **Holmes AJ**, **Yeo BTT**, **Turner GR**, **Dunbar RIM**, **Bzdok D.** The default network of the human brain is associated with perceived social isolation. *Nat Commun* 11: 6393, 2020 [Erratum in Nat Commun 12: 3202, 2021]. doi:10.1038/s41467-020-20039-w.
54. **Schurz M**, **Uddin LQ**, **Kanske P**, **Lamm C**, **Sallet J**, **Bernhardt BC**, **Mars RB**, **Bzdok D.** Variability in brain structure and function reflects lack of peer support. *Cereb Cortex* 31: 4612–4627, 2021. doi:10.1093/cercor/bhab109.
55. **Lindquist MA**, **Geuter S**, **Wager TD**, **Caffo BS.** Modular preprocessing pipelines can reintroduce artifacts into fMRI data. *Hum Brain Mapp* 40: 2358–2376, 2019. doi:10.1002/hbm.24528.
56. **Wang H-T**, **Smallwood J**, **Mourao-Miranda J**, **Xia CH**, **Satterthwaite TD**, **Bassett DS**, **Bzdok D.** Finding the needle in a high-dimensional haystack: canonical correlation analysis for neuroscientists. *NeuroImage* 216: 116745, 2020. doi:10.1016/j.neuroimage.2020.116745.
57. **Krishnan A**, **Williams LJ**, **McIntosh AR**, **Abdi H.** Partial least squares (PLS) methods for neuroimaging: a tutorial and review. *NeuroImage* 56: 455–475, 2011. doi:10.1016/j.neuroimage.2010.07.034.
58. **Winkler AM**, **Ridgway GR**, **Webster MA**, **Smith SM**, **Nichols TE.** Permutation inference for the general linear model. *NeuroImage* 92: 381–397, 2014. doi:10.1016/j.neuroimage.2014.01.060.
59. **Millard LAC**, **Davies NM**, **Gaunt TR**, **Davey Smith G**, **Tilling K.** Software application profile: PHESANT: a tool for performing automated phenome scans in UK Biobank. *Int J Epidemiol* 47: 29–35, 2018. doi:10.1093/ije/dyx204.
60. **Benjamini Y**, **Hochberg Y.** Controlling the false discovery rate: a practical and powerful approach to multiple testing. *J R Stat Soc B Methodol* 57: 289–300, 1995. doi:10.1111/j.2517-6161.1995.tb02031.x.
61. **Raizada RD**, **Richards TL**, **Meltzoff A**, **Kuhl PK.** Socioeconomic status predicts hemispheric specialisation of the left inferior frontal gyrus in young children. *NeuroImage* 40: 1392–1401, 2008. doi:10.1016/j.neuroimage.2008.01.021.
62. **Sha Z**, **Schijven D**, **Carrion-Castillo A**, **Joliot M**, **Mazoyer B**, **Fisher SE**, **Crivello F**, **Francks C.** The genetic architecture of structural left-right asymmetry of the human brain. *Nat Hum Behav* 5: 1226–1239, 2021. doi:10.1038/s41562-021-01069-w.

63. **Genovese CR**, **Lazar NA**, **Nichols T.** Thresholding of statistical maps in functional neuroimaging using the false discovery rate. *NeuroImage* 15: 870–878, 2002. doi:10.1006/nimg.2001.1037.
64. **King M**, **Hernandez-Castillo CR**, **Poldrack RA**, **Ivry RB**, **Diedrichsen J.** Functional boundaries in the human cerebellum revealed by a multi-domain task battery. *Nat Neurosci* 22: 1371–1378, 2019. doi:10.1038/s41593-019-0436-x.
65. **Margulies DS**, **Ghosh SS**, **Goulas A**, **Falkiewicz M**, **Huntenburg JM**, **Langs G**, **Bezgin G**, **Eickhoff SB**, **Castellanos FX**, **Petrides M**, **Jefferies E**, **Smallwood J.** Situating the default-mode network along a principal gradient of macroscale cortical organization. *Proc Natl Acad Sci USA* 113: 12574–12579, 2016. doi:10.1073/pnas.1608282113.
66. **Mesulam MM.** From sensation to cognition. *Brain* 121: 1013–1052, 1998. doi:10.1093/brain/121.6.1013.
67. **Guell X**, **Schmahmann JD**, **Gabrieli J**, **Ghosh SS.** Functional gradients of the cerebellum. *eLife* 7: e36652, 2018. doi:10.7554/eLife.36652.
68. **Spreng RN.** The fallacy of a "task-negative" network. *Front Psychol* 3: 145, 2012. doi:10.3389/fpsyg.2012.00145.
69. **Andrews-Hanna JR**, **Smallwood J**, **Spreng RN.** The default network and self-generated thought: component processes, dynamic control, and clinical relevance. *Ann N Y Acad Sci* 1316: 29–52, 2014. doi:10.1111/nyas.12360.
70. **Brissenden JA**, **Levin EJ**, **Osher DE**, **Halko MA**, **Somers DC.** Functional evidence for a cerebellar node of the dorsal attention network. *J Neurosci* 36: 6083–6096, 2016. doi:10.1523/JNEUROSCI.0344-16.2016.
71. **Fox MD**, **Snyder AZ**, **Vincent JL**, **Corbetta M**, **Van Essen DC**, **Raichle ME.** The human brain is intrinsically organized into dynamic, anticorrelated functional networks. *Proc Natl Acad Sci USA* 102: 9673–9678, 2005. doi:10.1073/pnas.0504136102.
72. **Chen CH**, **Newman LN**, **Stark AP**, **Bond KE**, **Zhang D**, **Nardone S**, **Vanderburg CR**, **Nadaf NM**, **Yao Z**, **Mutume K**, **Flaquer I**, **Lowell BB**, **Macosko EZ**, **Regehr WG.** A Purkinje cell to parabrachial nucleus pathway enables broad cerebellar influence over the forebrain. *Nat Neurosci* 26: 1929–1941, 2023. doi:10.1038/s41593-023-01462-w.
73. **Schmahmann JD**, **Sherman JC.** The cerebellar cognitive affective syndrome. *Brain* 121: 561–579, 1998. doi:10.1093/brain/121.4.561.
74. **Stoodley CJ**, **Valera EM**, **Schmahmann JD.** Functional topography of the cerebellum for motor and cognitive tasks: an fMRI study. *NeuroImage* 59: 1560–1570, 2012. doi:10.1016/j.neuroimage.2011.08.065.
75. **Stoodley CJ**, **Schmahmann JD.** Functional topography in the human cerebellum: a meta-analysis of neuroimaging studies. *Neuroimage* 44: 489–501, 2009. doi:10.1016/j.neuroimage.2008.08.039.
76. **Schmahmann JD**, **MacMore J**, **Vangel M.** Cerebellar stroke without motor deficit: clinical evidence for motor and non-motor domains within the human cerebellum. *Neuroscience* 162: 852–861, 2009. doi:10.1016/j.neuroscience.2009.06.023.
77. **Schmahmann JD.** Disorders of the cerebellum: ataxia, dysmetria of thought, and the cerebellar cognitive affective syndrome. *J Neuropsychiatry Clin Neurosci* 16: 367–378, 2004. doi:10.1176/jnp.16.3.367.
78. **Beaty RE**, **Silvia PJ**, **Nusbaum EC**, **Jauk E**, **Benedek M.** The roles of associative and executive processes in creative cognition. *Mem Cognit* 42: 1186–1197, 2014. doi:10.3758/s13421-014-0428-8.
79. **Beaty RE**, **Benedek M**, **Kaufman SB**, **Silvia PJ.** Default and executive network coupling supports creative idea production. *Sci Rep* 5: 10964, 2015. doi:10.1038/srep10964.
80. **Benedek M**, **Jauk E**, **Sommer M**, **Arendasy M**, **Neubauer AC.** Intelligence, creativity, and cognitive control: the common and differential involvement of executive functions in intelligence and creativity. *Intelligence* 46: 73–83, 2014. doi:10.1016/j.intell.2014.05.007.
81. **Wechsler D.** *The Measurement of Adult Intelligence*. Baltimore, MD: The Williams & Wilkins Company, 1944.
82. **Botez MI**, **Botez T**, **Elie R**, **Attig E.** Role of the cerebellum in complex human behavior. *Ital J Neurol Sci* 10: 291–300, 1989. doi:10.1007/BF02333774.
83. **Stoodley CJ**, **Schmahmann JD.** The cerebellum and language: evidence from patients with cerebellar degeneration. *Brain Lang* 110: 149–153, 2009. doi:10.1016/j.bandl.2009.07.006.
84. **Bolceková E**, **Mojzeš M**, **Van Tran Q**, **Kukal J**, **Ostrý S**, **Kulištõák P**, **Rusina R.** Cognitive impairment in cerebellar lesions: a logit model based on neuropsychological testing. *Cerebellum Ataxias* 4: 13, 2017. doi:10.1186/s40673-017-0071-9.
85. **Isaacs KR**, **Anderson BJ**, **Alcantara AA**, **Black JE**, **Greenough WT.** Exercise and the brain: angiogenesis in the adult rat cerebellum after vigorous physical activity and motor skill learning. *J Cereb Blood Flow Metab* 12: 110–119, 1992 [Erratum in J Cereb Blood Flow Metab 12: 533, 1992]. doi:10.1038/jcbfm.1992.14.
86. **Hamilton MT**, **Hamilton DG**, **Zderic TW.** Sedentary behavior as a mediator of type 2 diabetes. *Med Sport Sci* 60: 11–26, 2014. 10.1159/000357332.
87. **Bellettiere J**, **Healy GN**, **LaMonte MJ**, **Kerr J**, **Evenson KR**, **Rillamas-Sun E**, **Di C**, **Buchner DM**, **Hovell MF**, **LaCroix AZ.** Sedentary behavior and prevalent diabetes in 6,166 older women: the objective physical activity and cardiovascular health study. *J Gerontol A Biol Sci Med Sci* 74: 387–395, 2018. doi:10.1093/gerona/gly101.
88. **Strick PL**, **Dum RP**, **Fiez JA.** Cerebellum and nonmotor function. *Annu Rev Neurosci* 32: 413–434, 2009. doi:10.1146/annurev.neuro.31.060407.125606.
89. **Ito M.** Control of mental activities by internal models in the cerebellum. *Nat Rev Neurosci* 9: 304–313, 2008. doi:10.1038/nrn2332.
90. **Zhu J**, **Hasanbegović H**, **Liu LD**, **Gao Z**, **Li N.** Activity map of a cortico-cerebellar loop underlying motor planning. *Nat Neurosci* 26: 1916–1928, 2023. doi:10.1038/s41593-023-01453-x.
91. **Cajal SRY**, **Azoulay DL**, **Swanson N**, **Swanson IW.** *Histology of The Nervous System: Of Man and Vertebrates*. New York: Oxford University Press, 1995.
92. **Ito° M.** *The Cerebellum and Neural Control*. New York: Raven Press, 1984.
93. **Voogd J**, **Glickstein M.** The anatomy of the cerebellum. *Trends Neurosci* 21: 370–375, 1998. doi:10.1016/s0166-2236(98)01318-6.
94. **Schmahmann JD.** Dysmetria of thought: clinical consequences of cerebellar dysfunction on cognition and affect. *Trends Cogn Sci* 2: 362–371, 1998. doi:10.1016/s1364-6613(98)01218-2.
95. **Schmahmann JD.** The role of the cerebellum in affect and psychosis. *J Neurolinguistics* 13: 189–214, 2000. doi:10.1016/S0911-6044(00)00011-7.
96. **van Es DM**, **van der Zwaag W**, **Knapen T.** Topographic maps of visual space in the human cerebellum. *Curr Biol* 29: 1689–1694.e3, 2019. doi:10.1016/j.cub.2019.04.012.
97. **Guell X**, **D'Mello AM**, **Hubbard NA**, **Romeo RR**, **Gabrieli JDE**, **Whitfield-Gabrieli S**, **Schmahmann JD**, **Anteraper SA.** Functional territories of human dentate nucleus. *Cereb Cortex* 30: 2401–2417, 2020. doi:10.1093/cercor/bhz247.
98. **Xue A**, **Kong R**, **Yang Q**, **Eldaief MC**, **Angeli PA**, **DiNicola LM**, **Braga RM**, **Buckner RL**, **Yeo BTT.** The detailed organization of the human cerebellum estimated by intrinsic functional connectivity within the individual. *J Neurophysiol* 125: 358–384, 2021. doi:10.1152/jn.00561.2020.
99. **Brissenden JA**, **Tobyne SM**, **Osher DE**, **Levin EJ**, **Halko MA**, **Somers DC.** Topographic cortico-cerebellar networks revealed by visual attention and working memory. *Curr Biol* 28: 3364–3372.e5, 2018. doi:10.1016/j.cub.2018.08.059.
100. **Dixon ML**, **De La Vega A**, **Mills C**, **Andrews-Hanna J**, **Spreng RN**, **Cole MW**, **Christoff K.** Heterogeneity within the frontoparietal control network and its relationship to the default and dorsal attention networks. *Proc Natl Acad Sci USA* 115: E1598–E1607, 2018 [Erratum in Proc Natl Acad Sci USA 115: E3068, 2018]. doi:10.1073/pnas.1715766115.
101. **Corbetta M**, **Shulman GL.** Control of goal-directed and stimulus-driven attention in the brain. *Nat Rev Neurosci* 3: 201–215, 2002. doi:10.1038/nrn755.
102. **Buschman TJ**, **Kastner S.** From behavior to neural dynamics: an integrated theory of attention. *Neuron* 88: 127–144, 2015. doi:10.1016/j.neuron.2015.09.017.
103. **Ptak R.** The frontoparietal attention network of the human brain: action, saliency, and a priority map of the environment. *Neuroscientist* 18: 502–515, 2012. doi:10.1177/1073858411409051.
104. **Rosina A**, **Provini L.** Pontocerebellar system linking the two hemispheres by intracerebellar branching. *Brain Res* 296: 365–369, 1984. doi:10.1016/0006-8993(84)90075-1.
105. **Na J**, **Sugihara I**, **Shinoda Y.** The entire trajectories of single pontocerebellar axons and their lobular and longitudinal terminal distribution patterns in multiple aldolase C-positive compartments of the rat

cerebellar cortex. *J Comp Neurol* 527: 2488–2511, 2019. doi:10.1002/cne.24685.
106. **Voogd J.** Cerebellum and precerebellar nuclei. In: *The Human Nervous System*, edited by Paxinos G, Mai JK**.** Amsterdam: Elsevier Academic Press, 2004, p. 321–392.
107. **Schmahmann JD**, **Pandya DN.** Anatomical investigation of projections to the basis pontis from posterior parietal association cortices-inrhesus monkey. *J Comp Neurol* 289: 53–73, 1989. doi:10.1002/cne.902890105.
108. **Schmahmann JD**, **Pandya DN.** Projections to the basis pontis from the superior temporal sulcus and superior temporal region in the rhesus monkey. *J Comp Neurol* 308: 224–248, 1991. doi:10.1002/cne.903080209.
109. **Wiesendanger R**, **Wiesendanger M.** Cerebello-cortical linkage in the monkey as revealed by transcellular labeling with the lectin wheat germ agglutinin conjugated to the marker horseradish peroxidase. *Exp Brain Res* 59: 105–117, 1985. doi:10.1007/BF00237671.
110. **Chan-Palay V.** Efferent connections of the dentate nucleus. In: *Cerebellar Dentate Nucleus: Organization, Cytology and Transmitters*. Berlin, Heidelberg: Springer, 1977, p. 297–363.
111. **Flood S**, **Jansen J.** The efferent fibres of the cerebellar nuclei and their distribution on the cerebellar peduncles in the cat. *Cells Tissues Organs* 63: 137–166, 1966. doi:10.1159/000142786.
112. **Aumann TD**, **Horne MK.** Ramification and termination of single axons in the cerebellothalamic pathway of the rat. *J Comp Neurol* 376: 420–430, 1996. doi:10.1002/(SICI)1096-9861(19961216)376:3<420::AID-CNE5>3.0.CO;2-4.
113. **Cicirata F**, **Zappala A**, **Serapide MF**, **Parenti R**, **Panto MR**, **Paz C.** Different pontine projections to the two sides of the cerebellum. *Brain Res Brain Res Rev* 49: 280–294, 2005. doi:10.1016/j.brainresrev.2005.02.002.
114. **Serapide MF**, **Zappala A**, **Parenti R**, **Pantò MR**, **Cicirata F.** Laterality of the pontocerebellar projections in the rat. *Eur J Neurosci* 15: 1551–1556, 2002. doi:10.1046/j.1460-9568.2002.01993.x.
115. **Doron KW**, **Funk CM**, **Glickstein M.** Fronto-cerebellar circuits and eye movement control: a diffusion imaging tractography study of human cortico-pontine projections. *Brain Res* 1307: 63–71, 2010. doi:10.1016/j.brainres.2009.10.029.
116. **Axer H**, **Keyserlingk DG.** Mapping of fiber orientation in human internal capsule by means of polarized light and confocal scanning laser microscopy. *J Neurosci Methods* 94: 165–175, 2000. doi:10.1016/s0165-0270(99)00132-6.
117. **Ramnani N**, **Behrens TEJ**, **Johansen-Berg H**, **Richter MC**, **Pinsk MA**, **Andersson JLR**, **Rudebeck P**, **Ciccarelli O**, **Richter W**, **Thompson AJ**, **Gross CG**, **Robson MD**, **Kastner S**, **Matthews PM.** The evolution of prefrontal inputs to the cortico-pontine system: diffusion imaging evidence from macaque monkeys and humans. *Cereb Cortex* 16: 811–818, 2006. doi:10.1093/cercor/bhj024.
118. **Palesi F**, **De Rinaldis A**, **Castellazzi G**, **Calamante F**, **Muhlert N**, **Chard D**, **Tournier JD**, **Magenes G**, **D'Angelo E**, **Gandini Wheeler-Kingshott CAM.** Contralateral cortico-ponto-cerebellar pathways reconstruction in humans in vivo: implications for reciprocal cerebro-cerebellar structural connectivity in motor and non-motor areas. *Sci Rep* 7: 12841, 2017. doi:10.1038/s41598-017-13079-8.
119. **Keser Z**, **Hasan KM**, **Mwangi BI**, **Kamali A**, **Ucisik-Keser FE**, **Riascos RF**, **Yozbatiran N**, **Francisco GE**, **Narayana PA.** Diffusion tensor imaging of the human cerebellar pathways and their interplay with cerebral macrostructure. *Front Neuroanat* 9: 41, 2015. doi:10.3389/fnana.2015.00041.
120. **Karavasilis E**, **Christidi F**, **Velonakis G**, **Giavri Z**, **Kelekis NL**, **Efstathopoulos EP**, **Evdokimidis I**, **Dellatolas G.** Ipsilateral and contralateral cerebro-cerebellar white matter connections: A diffusion tensor imaging study in healthy adults. *J Neuroradiol* 46: 52–60, 2019. doi:10.1016/j.neurad.2018.07.004.
121. **Sokolov AA**, **Erb M**, **Grodd W**, **Pavlova MA.** Structural loop between the cerebellum and the superior temporal sulcus: evidence from diffusion tensor imaging. *Cereb Cortex* 24: 626–632, 2014. doi:10.1093/cercor/bhs346.
122. **Meola A**, **Comert A**, **Yeh FC**, **Sivakanthan S**, **Fernandez-Miranda JC.** The nondecussating pathway of the dentatorubrothalamic tract in humans: human connectome-based tractographic study and microdissection validation. *J Neurosurg* 124: 1406–1412, 2016. doi:10.3171/2015.4.JNS142741.
123. **Tacyildiz AE**, **Bilgin B**, **Gungor A**, **Ucer M**, **Karadag A**, **Tanriover N.** Dentate nucleus: connectivity-based anatomic parcellation based on superior cerebellar peduncle projections. *World Neurosurg* 152: e408–e428, 2021. doi:10.1016/j.wneu.2021.05.102.
124. **Petersen KJ**, **Reid JA**, **Chakravorti S**, **Juttukonda MR**, **Franco G**, **Trujillo P**, **Stark AJ**, **Dawant BM**, **Donahue MJ**, **Claassen DO.** Structural and functional connectivity of the nondecussating dentato-rubro-thalamic tract. *NeuroImage* 176: 364–371, 2018. doi:10.1016/j.neuroimage.2018.04.074.
125. **Kamali A**, **Kramer LA**, **Frye RE**, **Butler IJ**, **Hasan KM.** Diffusion tensor tractography of the human brain cortico-ponto-cerebellar pathways: a quantitative preliminary study. *J Magn Reson Imaging* 32: 809–817, 2010. doi:10.1002/jmri.22330.
126. **Habas C**, **Cabanis EA.** Anatomical parcellation of the brainstem and cerebellar white matter: a preliminary probabilistic tractography study at 3 T. *Neuroradiology* 49: 849–863, 2007. doi:10.1007/s00234-007-0267-4.
127. **Miall RC**, **Christensen LO.** The effect of rTMS over the cerebellum in normal human volunteers on peg-board movement performance. *Neurosci Lett* 371: 185–189, 2004. doi:10.1016/j.neulet.2004.08.067.
128. **Macher K**, **Böhringer A**, **Villringer A**, **Pleger B.** Cerebellar-parietal connections underpin phonological storage. *J Neurosci* 34: 5029–5037, 2014. doi:10.1523/JNEUROSCI.0106-14.2014.
129. **Cho SS**, **Yoon EJ**, **Bang SA**, **Park HS**, **Kim YK**, **Strafella AP**, **Kim SE.** Metabolic changes of cerebrum by repetitive transcranial magnetic stimulation over lateral cerebellum: a study with FDG PET. *Cerebellum* 11: 739–748, 2012. doi:10.1007/s12311-011-0333-7.
130. **Maldonado T**, **Jackson TB**, **Bernard JA.** Anodal cerebellar stimulation increases cortical activation: evidence for cerebellar scaffolding of cortical processing. *Hum Brain Mapp* 44: 1666–1682, 2023. doi:10.1002/hbm.26166.
131. **Igelstrom KM**, **Webb TW**, **Graziano MSA.** Functional connectivity between the temporoparietal cortex and cerebellum in autism spectrum disorder. *Cereb Cortex* 27: 2617–2627, 2017. doi:10.1093/cercor/bhw079.
132. **Bernard JA**, **Seidler RD**, **Hassevoort KM**, **Benson BL**, **Welsh RC**, **Wiggins JL**, **Jaeggi SM**, **Buschkuehl M**, **Monk CS**, **Jonides J**, **Peltier SJ.** Resting state cortico-cerebellar functional connectivity networks: a comparison of anatomical and self-organizing map approaches. *Front Neuroanat* 6: 31, 2012. doi:10.3389/fnana.2012.00031.
133. **Bernard JA**, **Peltier SJ**, **Benson BL**, **Wiggins JL**, **Jaeggi SM**, **Buschkuehl M**, **Jonides J**, **Monk CS**, **Seidler RD.** Dissociable functional networks of the human dentate nucleus. *Cereb Cortex* 24: 2151–2159, 2014. doi:10.1093/cercor/bht065.
134. **Jiang R**, **Westwater ML**, **Noble S**, **Rosenblatt M**, **Dai W**, **Qi S**, **Sui J**, **Calhoun VD**, **Scheinost D.** Associations between grip strength, brain structure, and mental health in > 40,000 participants from the UK Biobank. *BMC Med* 20: 286, 2022. doi:10.1186/s12916-022-02490-2.
135. **Li W**, **Li Y**, **Chen Y**, **Yue L**, **Xiao S.** Association between physical exercise, executive function, and cerebellar cortex: a cross-sectional study among the elderly in Chinese communities. *Front Aging Neurosci* 14: 975329, 2022. doi:10.3389/fnagi.2022.975329.
136. **Ben-Soussan TD**, **Berkovich-Ohana A**, **Piervincenzi C**, **Glicksohn J**, **Carducci F.** Embodied cognitive flexibility and neuroplasticity following Quadrato Motor Training. *Front Psychol* 6: 1021, 2015. doi:10.3389/fpsyg.2015.01021.
137. **Callow DD**, **Won J**, **Pena GS**, **Jordan LS**, **Arnold-Nedimala NA**, **Kommula Y**, **Nielson KA**, **Smith JC.** Exercise training-related changes in cortical gray matter diffusivity and cognitive function in mild cognitive impairment and healthy older adults. *Front Aging Neurosci* 13: 645258, 2021. doi:10.3389/fnagi.2021.645258.
138. **Won J**, **Faroqi-Shah Y**, **Callow DD**, **Williams A**, **Awoyemi A**, **Nielson KA**, **Smith JC.** Association between greater cerebellar network connectivity and improved phonemic fluency performance after exercise training in older adults. *Cerebellum* 20: 542–555, 2021. doi:10.1007/s12311-020-01218-3.
139. **Lopez-Lopez C**, **LeRoith D**, **Torres-Aleman I.** Insulin-like growth factor I is required for vessel remodeling in the adult brain. *Proc Natl Acad Sci USA* 101: 9833–9838, 2004. doi:10.1073/pnas.0400337101.
140. **Black JE**, **Isaacs KR**, **Anderson BJ**, **Alcantara AA**, **Greenough WT.** Learning causes synaptogenesis, whereas motor activity causes angiogenesis, in cerebellar cortex of adult rats. *Proc Natl Acad Sci USA* 87: 5568–5572, 1990. doi:10.1073/pnas.87.14.5568.

141. **Hashimoto M**, **Yamanaka A**, **Kato S**, **Tanifuji M**, **Kobayashi K**, **Yaginuma H.** Anatomical evidence for a direct projection from Purkinje cells in the mouse cerebellar vermis to medial parabrachial nucleus. *Front Neural Circuits* 12: 6, 2018. doi:10.3389/fncir.2018.00006.
142. **Nisimaru N**, **Katayama S.** Projection of cardiovascular afferents to the lateral nodulus-uvula of the cerebellum in rabbits. *Neurosci Res* 21: 343–350, 1995. doi:10.1016/0168-0102(94)00872-d.
143. **Nisimaru N.** Cardiovascular modules in the cerebellum. *Jpn J Physiol* 54: 431–448, 2004 [Erratum in Jpn J Physiol 55: 79, 2005]. doi:10.2170/jjphysiol.54.431.
144. **Nisimaru N**, **Mittal C**, **Shirai Y**, **Sooksawate T**, **Anandaraj P**, **Hashikawa T**, **Nagao S**, **Arata A**, **Sakurai T**, **Yamamoto M**, **Ito M.** Orexin-neuromodulated cerebellar circuit controls redistribution of arterial blood flows for defense behavior in rabbits. *Proc Natl Acad Sci USA* 110: 14124–14131, 2013. doi:10.1073/pnas.1312804110.
145. **Reis DJ**, **Doba N**, **Nathan MA.** Predatory attack, grooming, and consummatory behaviors evoked by electrical stimulation of cat cerebellar nuclei. *Science* 182: 845–847, 1973. doi:10.1126/science.182.4114.845.
146. **Rasheed BMA**, **Manchanda SK**, **Anand BK.** Effects of the stimulation of paleocerebellum on certain vegetative functions in the cat. *Brain Res* 20: 293–308, 1970. doi:10.1016/0006-8993(70)90296-9.
147. **Zanchetti A**, **Zoccolini A.** Autonomic hypothalamic outbursts elicited by cerebellar stimulation. *J Neurophysiol* 17: 475–483, 1954. doi:10.1152/jn.1954.17.5.475.
148. **Moruzzi G.** Sham rage and localized autonomic responses elicited by cerebellar stimulation in the acute thalamic cat. *Proc XVII Int Physiol Con* 114–115, 1947.
149. **Martner J.** Cerebellar influences on autonomic mechanisms. An experimental study in the cat with special reference to the fastigial nucleus. *Acta Physiol Scand* 425: 1–42, 1975.
150. **Canto CB**, **Onuki Y**, **Bruinsma B**, **van der Werf YD**, **De Zeeuw CI.** The sleeping cerebellum. *Trends Neurosci* 40: 309–323, 2017. doi:10.1016/j.tins.2017.03.001.
151. **DelRosso LM**, **Hoque R.** The cerebellum and sleep. *Neurol Clin* 32: 893–900, 2014. doi:10.1016/j.ncl.2014.07.003.
152. **Pedroso JL**, **Braga-Neto P**, **Felício AC**, **Aquino CC**, **Prado LB**, **Prado GFd**, **Barsottini OG.** Sleep disorders in cerebellar ataxias. *Arq Neuropsiquiatr* 69: 253–257, 2011. doi:10.1590/s0004-282x2011000200021.
153. **Taki Y**, **Hashizume H**, **Sassa Y**, **Takeuchi H**, **Asano M**, **Asano K**, **Kotozaki Y**, **Nouchi R**, **Wu K**, **Fukuda H**, **Kawashima R.** Correlation among body height, intelligence, and brain gray matter volume in healthy children. *NeuroImage* 59: 1023–1027, 2012. doi:10.1016/j.neuroimage.2011.08.092.
154. **Hara D**, **Maki F**, **Tanaka S**, **Sasaki R**, **Hasegawa Y.** MRI-based cerebellar volume measurements correlate with the International Cooperative Ataxia Rating Scale score in patients with spinocerebellar degeneration or multiple system atrophy. *Cerebellum Ataxias* 3: 14, 2016. doi:10.1186/s40673-016-0052-4.
155. **Hutchinson S**, **Lee LH-L**, **Gaab N**, **Schlaug G.** Cerebellar volume of musicians. *Cereb Cortex* 13: 943–949, 2003. doi:10.1093/cercor/13.9.943.
156. **Park IS**, **Lee KJ**, **Han JW**, **Lee NJ**, **Lee WT**, **Park KA**, **Rhyu IJ.** Experience-dependent plasticity of cerebellar vermis in basketball players. *Cerebellum* 8: 334–339, 2009. doi:10.1007/s12311-009-0100-1.
157. **Taki Y**, **Kinomura S**, **Sato K**, **Inoue K**, **Goto R**, **Okada K**, **Uchida S**, **Kawashima R**, **Fukuda H.** Relationship between body mass index and gray matter volume in 1,428 healthy individuals. *Obesity (Silver Spring)* 16: 119–124, 2008. doi:10.1038/oby.2007.4.
158. **Kurth F**, **Levitt JG**, **Phillips OR**, **Luders E**, **Woods RP**, **Mazziotta JC**, **Toga AW**, **Narr KL.** Relationships between gray matter, body mass index, and waist circumference in healthy adults. *Hum Brain Mapp* 34: 1737–1746, 2013. doi:10.1002/hbm.22021.
159. **Pannacciulli N**, **Del Parigi A**, **Chen K**, **Le DSN**, **Reiman EM**, **Tataranni PA.** Brain abnormalities in human obesity: a voxel-based morphometric study. *Neuroimage* 31: 1419–1425, 2006. doi:10.1016/j.neuroimage.2006.01.047.
160. **Walther K**, **Birdsill AC**, **Glisky EL**, **Ryan L.** Structural brain differences and cognitive functioning related to body mass index in older females. *Hum Brain Mapp* 31: 1052–1064, 2010. doi:10.1002/hbm.20916.
161. **Weise CM**, **Thiyyagura P**, **Reiman EM**, **Chen K**, **Krakoff J.** Fat-free body mass but not fat mass is associated with reduced gray matter volume of cortical brain regions implicated in autonomic and homeostatic regulation. *NeuroImage* 64: 712–721, 2013. doi:10.1016/j.neuroimage.2012.09.005.
162. **Takeuchi H**, **Taki Y**, **Hashizume H**, **Asano K**, **Asano M**, **Sassa Y**, **Yokota S**, **Kotozaki Y**, **Nouchi R**, **Kawashima R.** The impact of television viewing on brain structures: cross-sectional and longitudinal analyses. *Cereb Cortex* 25: 1188–1197, 2015. doi:10.1093/cercor/bht315.
163. **Takeuchi H**, **Kawashima R.** Effects of television viewing on brain structures and risk of dementia in the elderly: longitudinal analyses. *Front Neurosci* 17: 984919, 2023. doi:10.3389/fnins.2023.984919.
164. **Dougherty RJ**, **Hoang TD**, **Launer LJ**, **Jacobs DR**, **Sidney S**, **Yaffe K.** Long-term television viewing patterns and gray matter brain volume in midlife. *Brain Imaging Behav* 16: 637–644, 2022. doi:10.1007/s11682-021-00534-4.
165. **Grøntved A**, **Hu FB.** Television viewing and risk of type 2 diabetes, cardiovascular disease, and all-cause mortality: a meta-analysis. *JAMA* 305: 2448–2455, 2011. doi:10.1001/jama.2011.812.
166. **Patterson F**, **Mitchell JA**, **Dominick G**, **Lozano AJ**, **Huang L**, **Hanlon AL.** Does meeting physical activity recommendations ameliorate association between television viewing with cardiovascular disease risk? A cross-sectional, population-based analysis. *BMJ Open* 10: e036507, 2020. doi:10.1136/bmjopen-2019-036507.
167. **Ekelund U**, **Steene-Johannessen J**, **Brown WJ**, **Fagerland MW**, **Owen N**, **Powell KE**, **Bauman A**, **Lee IM**; **Lancet Physical Activity Series 2 Executive Committe; Lancet Sedentary Behaviour Working Group.** Does physical activity attenuate, or even eliminate, the detrimental association of sitting time with mortality? A harmonised meta-analysis of data from more than 1 million men and women. *Lancet* 388: 1302–1310, 2016 [Erratum in *Lancet* 388: e6, 2016]. doi:10.1016/S0140-6736(16)30370-1.
168. **Chomistek AK**, **Manson JE**, **Stefanick ML**, **Lu B**, **Sands-Lincoln M**, **Going SB**, **Garcia L**, **Allison MA**, **Sims ST**, **LaMonte MJ**, **Johnson KC**, **Eaton CB.** Relationship of sedentary behavior and physical activity to incident cardiovascular disease: results from the Women's Health Initiative. *J Am Coll Cardiol* 61: 2346–2354, 2013. doi:10.1016/j.jacc.2013.03.031.
169. **Crichton GE**, **Alkerwi A.** Physical activity, sedentary behavior time and lipid levels in the Observation of Cardiovascular Risk Factors in Luxembourg Study. *Lipids Health Dis* 14: 87, 2015. doi:10.1186/s12944-015-0085-3.
170. **Sniderman AD**, **Navar AM**, **Thanassoulis G.** Apolipoprotein B vs low-density lipoprotein cholesterol and non–high-density lipoprotein cholesterol as the primary measure of apolipoprotein B lipoprotein-related risk: the debate is over. *JAMA Cardiol* 7: 257–258, 2022. doi:10.1001/jamacardio.2021.5080.
171. **Contois JH**, **Langlois MR**, **Cobbaert C**, **Sniderman AD.** Standardization of apolipoprotein B, LDL-cholesterol, and non-HDL-cholesterol. *J Am Heart Assoc* 12: e030405, 2023. doi:10.1161/JAHA.123.030405.
172. **Sniderman AD**, **Williams K**, **Contois JH**, **Monroe HM**, **McQueen MJ**, **Graaf J**, **Furberg CD.** A meta-analysis of low-density lipoprotein cholesterol, non-high-density lipoprotein cholesterol, and apolipoprotein B as markers of cardiovascular risk. *Circ Cardiovasc Qual Outcomes* 4: 337–345, 2011. doi:10.1161/CIRCOUTCOMES.110.959247.
173. **Shah H**, **Eisenbarth S**, **Tormey CA**, **Siddon AJ.** Behind the scenes with basophils: an emerging therapeutic target. *Immunother Adv* 1: ltab008, 2021. doi:10.1093/immadv/ltab008.
174. **Pizzolo F**, **Castagna A**, **Olivieri O**, **Girelli D**, **Friso S**, **Stefanoni F**, **Udali S**, **Munerotto V**, **Baroni M**, **Cetera V**, **Luciani GB**, **Faggian G**, **Bernardi F**, **Martinelli N.** Basophil blood cell count is associated with enhanced factor ii plasma coagulant activity and increased risk of mortality in patients with stable coronary artery disease: not only neutrophils as prognostic marker in ischemic heart disease. *J Am Heart Assoc* 10: e018243, 2021. doi:10.1161/JAHA.120.018243.
175. **Zhang S-S**, **Yang X-J**, **Ma Q-H**, **Xu Y**, **Chen X**, **Wang P**, **Pan C-W.** Leukocyte related parameters in older adults with metabolically healthy and unhealthy overweight or obesity. *Sci Rep* 11: 4652, 2021. doi:10.1038/s41598-021-84367-7.
176. **Juonala M**, **Viikari JSA**, **Kähönen M**, **Taittonen L**, **Laitinen T**, **Hutri-Kähönen N**, **Lehtimäki T**, **Jula A**, **Pietikäinen M**, **Jokinen E**, **Telama**

R, **Räsänen L**, **Mikkilä V**, **Helenius H**, **Kivimäki M**, **Raitakari OT.** Lifetime risk factors and progression of carotid atherosclerosis in young adults: the Cardiovascular Risk in Young Finns Study. *Eur Heart J* 31: 1745–1751, 2010. doi:10.1093/eurheartj/ehq141.

177. **Liu B**, **Ni J**, **Shi M**, **Bai L**, **Zhan C**, **Lu H**, **Wu Y**, **Tu J**, **Ning X**, **Hao J**, **Wang J.** Carotid intima-media thickness and its association with conventional risk factors in low-income adults: a population-based cross-sectional study in China. *Sci Rep* 7: 41500, 2017. doi:10.1038/srep41500.
178. **Zhang L**, **Fan F**, **Qi L**, **Jia J**, **Yang Y**, **Li J**, **Zhang Y.** The association between carotid intima-media thickness and new-onset hypertension in a Chinese community-based population. *BMC Cardiovasc Disord* 19: 269, 2019. doi:10.1186/s12872-019-1266-1.
179. **Ferreira JP**, **Girerd N**, **Bozec E**, **Machu JL**, **Boivin JM**, **London GM**, **Zannad F**, **Rossignol P.** Intima-media thickness is linearly and continuously associated with systolic blood pressure in a population-based cohort (STANISLAS Cohort Study). *J Am Heart Assoc* 5: e003529, 2016. doi:10.1161/JAHA.116.003529.
180. **Anderson DR**, **Davidson MC.** Receptive versus interactive video screens: a role for the brain's default mode network in learning from media. *Comput Hum Behav* 99: 168–180, 2019. doi:10.1016/j.chb.2019.05.008.
181. **Raichle ME.** The neural correlates of consciousness: an analysis of cognitive skill learning. *Philos Trans R Soc Lond B Biol Sci* 353: 1889–1901, 1998. doi:10.1098/rstb.1998.0341.
182. **Landhuis CE**, **Poulton R**, **Welch D**, **Hancox RJ.** Does childhood television viewing lead to attention problems in adolescence? Results from a prospective longitudinal study. *Pediatrics* 120: 532–537, 2007. doi:10.1542/peds.2007-0978.
183. **Christakis DA**, **Zimmerman FJ**, **DiGiuseppe DL**, **McCarty CA.** Early television exposure and subsequent attentional problems in children. *Pediatrics* 113: 708–713, 2004. doi:10.1542/peds.113.4.708.
184. **Johnson JG**, **Cohen P**, **Kasen S**, **Brook JS.** Extensive television viewing and the development of attention and learning difficulties during adolescence. *Arch Pediatr Adolesc Med* 161: 480–486, 2007. doi:10.1001/archpedi.161.5.480.
185. **Yang E**, **Milisav F**, **Kopal J**, **Holmes AJ**, **Mitsis GD**, **Misic B**, **Finn ES**, **Bzdok D.** The default network dominates neural responses to evolving movie stories. *Nat Commun* 14: 4197, 2023. doi:10.1038/s41467-023-39862-y.
186. **Cochrane A**, **Simmering V**, **Green CS.** Fluid intelligence is related to capacity in memory as well as attention: evidence from middle childhood and adulthood. *PLoS One* 14: e0221353, 2019. doi:10.1371/journal.pone.0221353.
187. **Burgess PW**, **Quayle A**, **Frith CD.** Brain regions involved in prospective memory as determined by positron emission tomography. *Neuropsychologia* 39: 545–555, 2001. doi:10.1016/S0028-3932(00)00149-4.
188. **Kliegel M**, **Martin M**, **McDaniel MA**, **Einstein GO.** Complex prospective memory and executive control of working memory: a process model. *Psychologische Beitrage* 44: 303–318, 2002.
189. **Engle RW**, **Tuholski SW**, **Laughlin JE**, **Conway ARA.** Working memory, short-term memory, and general fluid intelligence: a latent-variable approach. *J Exp Psychol Gen* 128: 309–331, 1999. doi:10.1037//0096-3445.128.3.309.
190. **Wong TT-Y**, **Liu D.** The association between visual attention and arithmetic competence: The mediating role of enumeration. *J Exp Child Psychol* 196: 104864, 2020. doi:10.1016/j.jecp.2020.104864.
191. **Chun JW**, **Choi J**, **Kim JY**, **Cho H**, **Ahn KJ**, **Nam JH**, **Choi JS**, **Kim DJ.** Altered brain activity and the effect of personality traits in excessive smartphone use during facial emotion processing. *Sci Rep* 7: 12156, 2017. doi:10.1038/s41598-017-08824-y.
192. **Tymofiyeva O**, **Yuan JP**, **Kidambi R**, **Huang CY**, **Henje E**, **Rubinstein ML**, **Jariwala N**, **Max JE**, **Yang TT**, **Xu D.** Neural correlates of smartphone dependence in adolescents. *Front Hum Neurosci* 14: 564629, 2020. doi:10.3389/fnhum.2020.564629.
193. **Horvath J**, **Mundinger C**, **Schmitgen MM**, **Wolf ND**, **Sambataro F**, **Hirjak D**, **Kubera KM**, **Koenig J**, **Christian Wolf R.** Structural and functional correlates of smartphone addiction. *Addict Behav* 105: 106334, 2020. doi:10.1016/j.addbeh.2020.106334.
194. **Wang Y**, **Zou Z**, **Song H**, **Xu X**, **Wang H**, **d'Oleire Uquillas F**, **Huang X.** Altered gray matter volume and white matter integrity in college students with mobile phone dependence. *Front Psychol* 7: 597, 2016. doi:10.3389/fpsyg.2016.00597.
195. **Ha M**, **Park SH**, **Park I**, **Kim T**, **Lee J**, **Kim M**, **Kwon JS.** Aberrant cortico-thalamo-cerebellar network interactions and their association with impaired cognitive functioning in patients with schizophrenia. *Schizophrenia (Heidelb)* 9: 50, 2023. doi:10.1038/s41537-023-00375-8.
196. **Nicoletti V**, **Cecchi P**, **Pesaresi I**, **Frosini D**, **Cosottini M**, **Ceravolo R.** Cerebello-thalamo-cortical network is intrinsically altered in essential tremor: evidence from a resting state functional MRI study. *Sci Rep* 10: 16661, 2020. doi:10.1038/s41598-020-73714-9.
197. **Bostan AC**, **Strick PL.** The cerebellum and basal ganglia are interconnected. *Neuropsychol Rev* 20: 261–270, 2010. doi:10.1007/s11065-010-9143-9.
198. **Bostan AC**, **Dum RP**, **Strick PL.** Cerebellar networks with the cerebral cortex and basal ganglia. *Trends Cogn Sci* 17: 241–254, 2013. doi:10.1016/j.tics.2013.03.003.
199. **Bostan AC**, **Strick PL.** The basal ganglia and the cerebellum: nodes in an integrated network. *Nat Rev Neurosci* 19: 338–350, 2018. doi:10.1038/s41583-018-0002-7.
200. **Zhi D**, **Jiang R**, **Pearlson G**, **Fu Z**, **Qi S**, **Yan W**, **Feng A**, **Xu M**, **Calhoun V**, **Sui J.** Triple interactions between the environment, brain, and behavior in children: an ABCD study. *Biol Psychiatry* 95: 828–838, 2024. doi:10.1016/j.biopsych.2023.12.019.
201. **Hoshi E**, **Tremblay L**, **Féger J**, **Carras PL**, **Strick PL.** The cerebellum communicates with the basal ganglia. *Nat Neurosci* 8: 1491–1493, 2005. doi:10.1038/nn1544.